Molecular basis for inhibition of *Plasmodium vivax* reticulocyte invasion by a vaccine-induced broadly neutralising human monoclonal antibody

Thomas. A. Rawlinson[1#], Natalie M. Barber[2#], Franziska Mohring[3], Jee Sun Cho[1], Varakorn Kosaisavee[4], Samuel F. Gérard[2], Daniel G. W. Alanine[1], Geneviève M. Labbé[1], Sean C. Elias[1], Sarah E. Silk[1], Doris Quinkert[1], Jing Jin[1], Jennifer M. Marshall[1], Ruth O. Payne[1], Bruce Russell[5], Laurent Rénia[6], François H. Nosten[7], Robert W. Moon[3], Matthew K. Higgins[2]* and Simon J. Draper[1]*.

[1] The Jenner Institute, University of Oxford, Old Road Campus Research Building, Oxford, OX3 7DQ, UK.

[2] Department of Biochemistry, University of Oxford, South Parks Road, Oxford, OX1 3QU, UK.

[3] Department of Immunology and Infection, Faculty of Infectious and Tropical Diseases, London School of Hygiene and Tropical Medicine, London WC1E 7HT, UK.

[4] Faculty of Public Health, Mahidol University, Bangkok, Thailand.

[5] Department of Microbiology and Immunology, School of Biomedical Sciences, University of Otago, Dunedin, New Zealand.

[6] Singapore Immunology Network (SIgN), A*STAR, 8A Biomedical Grove, Singapore 138648, Singapore.

[7] Shoklo Malaria Research Unit, Mahidol-Oxford Tropical Medicine Research Unit, Faculty of Tropical Medicine, Mahidol University, 68/30 Bantung Road, Mae Sot 63110, Thailand.

[#] Contributed equally

* Address correspondence and requests for materials to: simon.draper@ndm.ox.ac.uk (S.J.D.) and matthew.higgins@bioch.ox.ac.uk (M.K.H.).

ABSTRACT

The most widespread form of malaria is caused by *Plasmodium vivax*. To replicate, this parasite must invade immature red blood cells, through a process which requires interaction of the *Plasmodium vivax* Duffy binding protein, *Pv*DBP with its human receptor, the Duffy antigen receptor for chemokines, DARC. Naturally acquired antibodies that inhibit this interaction associate with clinical immunity, suggesting *Pv*DBP as a leading candidate for inclusion in a vaccine to prevent malaria due to *Plasmodium vivax*. Here, we isolated a panel of monoclonal antibodies from human volunteers immunised in the first clinical vaccine trial of *Pv*DBP. We screened their ability to prevent *Pv*DBP from binding to DARC, and their capacity to block red blood cell invasion by a transgenic *Plasmodium knowlesi* parasite genetically modified to express *Pv*DBP and to prevent reticulocyte invasion by multiple clinical isolates of *Plasmodium vivax*. This identified a broadly neutralising human monoclonal antibody which inhibited invasion of all tested strains of *Plasmodium vivax*. Finally, we determined the structure of a complex of this antibody bound to *Pv*DBP, revealing the molecular basis for inhibition. These findings will guide future vaccine design strategies and open up possibilities for testing the prophylactic use of such an antibody.

INTRODUCTION

In large parts of the world, *Plasmodium vivax* is the dominant species causing human malaria [1, 2]. An effective blood-stage vaccine would reduce morbidity, lower blood-stage asexual and sexual parasite densities and aid progress towards elimination. The symptoms of malaria occur as the parasites invade, replicate within and burst out of the red blood cells (RBC) of infected individuals. *Plasmodium vivax* parasites invade immature RBC, selecting reticulocytes that express the transferrin receptor CD71 [3, 4]. Important in this invasion process is the parasite surface protein, *Plasmodium vivax* Duffy-binding protein, *Pv*DBP, which interacts with the Duffy antigen receptor for chemokines, DARC/Fy, on the surface of reticulocytes, in a process essential for invasion [5, 6]. Consistent with this, genetic knockout of the orthologous DBPα gene from the closely-related simian malaria *Plasmodium knowlesi* also prevents invasion of Duffy-positive erythrocytes *in vitro* [7] and antibodies that target PkDBP can block invasion of RBC by *Plasmodium knowlesi* [8]. Moreover, a human polymorphism which results in Duffy-negative erythrocytes [9] is widespread across Africa and is associated with protection from *Plasmodium vivax* infection [10]. This leads to low levels of vivax-malaria across much of the continent [11] and highlights *Pv*DBP as the most promising candidate for inclusion in a vaccine to prevent *Plasmodium vivax* [12].

*Pv*DBP has been divided into six distinct regions, with the DARC binding site mapped to a ~350 amino acid residue domain known as Region II, *Pv*DBPII, which takes the form of a Duffy-binding-like (DBL) domain [6]. The first structure of a DBL domain was that from the *P. knowlesi* orthologue of *Pv*DBPII [5] and was split into three regions, known as subdomains 1-3 [5]. *Pv*DBPII binds to the sixty-residue extracellular N-terminal ectodomain of DARC, in an interaction which requires DARC to be post-translationally modified by sulphation of two tyrosine residues, Tyr30 and Try41 [13, 14]. Nevertheless, the interaction between *Pv*DBPII and DARC is only partially understood. Structural studies of *Pv*DBPII show the domain to form dimers in both solution and in a crystal [13]. In addition, structures of *Pv*DBPII crystallised in the presence of the ectodomain of DARC, reveal an ordered 11-

68 residue helical peptide ($DARC_{19-30}$), which lies close to the *Pv*DBPII dimer interface in subdomain 2
69 [15]. However, the DARC protein used in these studies was not tyrosine-sulphated and sulphated
70 Tyr41, which cannot be seen in this study, was previously shown to be essential for high affinity
71 *Pv*DBPII binding [14]. Indeed, mapping residues identified by mutagenesis onto the structure of
72 *Pv*DBPII reveals an additional patch on subdomain 2 proposed to contribute to DARC binding [16, 17]
73 and it is likely that the DARC binding site spans much of the surface of subdomain 2 and includes
74 both this patch and the region that interacts with the helical $DARC_{19-30}$ peptide.
75
76 Development of *Pv*DBPII-based vaccine candidates has progressed through pre-clinical studies to the
77 first Phase I human clinical trials, both recently reported [18, 19]. Immunisation of mice, rabbits and
78 non-human primates using *Pv*DBPII-based vaccines induces the production of inhibitory antibodies
79 that block recombinant *Pv*DBPII:DARC *in vitro* binding [20, 21]. However, challenges in sustaining
80 *Plasmodium vivax* in long-term culture [22] have prevented these antibodies from being robustly
81 tested in standardised functional growth inhibition assays, as is traditionally performed for vaccines
82 targeting *Plasmodium falciparum* [12]. Nevertheless, in humans, the presence of high-titres of
83 naturally-acquired antibodies that target *Pv*DBPII and prevent DARC binding *in vitro* are associated
84 with reduced risk of *Plasmodium vivax* infection [23], as well as lower parasite densities following
85 invasion and decreased risk of clinical malaria [24, 25]. Encouragingly, in a recent Phase Ia clinical
86 trial, immunisation of human volunteers using recombinant viral vectors expressing *Pv*DBPII induced
87 strain-transcending antibodies which prevented recombinant *Pv*DBPII from binding to DARC [19],
88 confirming for the first time that such antibodies could be raised by human vaccination.
89
90 Several studies have investigated the molecular basis for antibody-mediated inhibition of DARC
91 binding by *Pv*DBPII [13, 15, 26, 27]. Screening a linear peptide array with non-inhibitory and
92 inhibitory human serum has identified peptides which recognise antibodies found specifically in
93 inhibitory serum [27]. These peptides are located within subdomain 2, in the regions involved in

94 *Pv*DBPII dimerisation and $DARC_{19-30}$ peptide binding [15]. These data suggest that antibodies which
95 directly block dimerisation and DARC binding are desirable. In addition, a study of monoclonal
96 antibodies (mAbs) derived from *Pv*DBPII-immunised mice used structural studies and mass-
97 spectrometry based mapping approaches to identify three epitopes for antibodies shown to block
98 DARC binding *in vitro* [26]. Surprisingly, these epitopes are located on subdomain 3 of *Pv*DBPII,
99 distant from the DARC binding site.
100
101 In order to understand the epitopes for human inhibitory antibodies, and to guide future structure-
102 guided immunogen development, we have now cloned a panel of antibodies from *Pv*DBPII
103 immunised human volunteers. We have determined their ability to inhibit the binding of
104 recombinant *Pv*DBPII to DARC *in vitro*, as well as their capacity to neutralise parasite invasion in two
105 distinct parasite-based functional assays. Our data provide important insight into these different *in*
106 *vitro* readouts of antibody function and, furthermore, have led to the structural characterisation of
107 an epitope for an antibody that shows broadly neutralising activity against parasite invasion.
108

RESULTS

Cloning of a panel of vaccine-induced human monoclonal antibodies that bind to *Pv*DBPII

Anti-*Pv*DBPII mAbs were isolated from the antibody-secreting cells of immunised volunteers enrolled in a first-in-human Phase Ia clinical trial of a *Pv*DBPII-based vaccine delivered using recombinant chimpanzee adenovirus and poxvirus viral vectors [19]. Variable region (VR)-coding genes were isolated by RT-PCR and PCR and cloned into a human IgG1 scaffold. Cognate heavy-chain and light-chain plasmids were expressed together in HEK293 cells and vaccine antigen-specificity was confirmed by supernatant reactivity to a *Pv*DBPII protein comprising amino acids D194 to T521.

Ten genetically distinct mAbs were isolated (**Table S1**). Aligning them with the most similar germline VR genes in IgBLAST [28] showed little non-germline sequence, suggesting the viral vectored vaccine regimen drives minimal somatic hypermutation in humans. The monovalent binding affinity of each mAb was assessed by surface plasmon resonance (SPR) (**Figure 1A-D** and **Table S2**). Affinities were in the low nanomolar to high picomolar range, likely owing to the use of a stringent ELISA selection process during mAb isolation.

To understand the relationship between binding site and function, mAbs were tested in pairs for their ability to bind simultaneously to biotinylated *Pv*DBPII by Biolayer Interferometry (BLI) (**Figure 1E,F**). This defined two distinct epitope bins containing mAbs which bind overlapping epitopes, as well as three mAbs with distinct non-overlapping epitopes (**Figure 1G**).

To characterise the ability of the human mAbs to inhibit binding of *Pv*DBPII to DARC, they were tested *in vitro* in an ELISA-based binding inhibition assay [29]. The effect of *Pv*DBPII polymorphism on mAb recognition was assessed by testing their effect on the binding of the N-terminal DARC ectodomain to a panel of five sequence-divergent *Pv*DBPII proteins [19] (**Figure 2**, **Figure S1**). Most

mAbs showed differential binding inhibition, with only two (DB2 and DB9) inhibiting the DARC binding of all five *Pv*DBPII variant alleles (**Figure 2**).

Assessing the neutralisation of parasite invasion by the antibody panel

To characterise the ability of the human mAbs to block merozoite entry into RBC, assays of growth inhibition activity (GIA) were performed. A novel *Plasmodium knowlesi* line was used that has been adapted to long-term *in vitro* culture in human RBC [30] and in which the native PkDBPα gene had been replaced by the *Pv*DBP gene (Mohring F *et al*., submitted). *Plasmodium knowlesi* is also dependent on the DARC receptor for RBC invasion, but unlike *Plasmodium vivax*, it has three DBP genes; PkDBPα, PkDBPβ and PkDBPγ [31]. PkDBPβ and PkDBPγ are thought to be required for invasion of rhesus RBC whereas PkDBPα is essential for invasion of human RBC [7, 32, 33]. The ten mAbs were thus assayed for growth inhibition against five *Plasmodium knowlesi* lines: First, the original human-RBC adapted PkA1H1 strain [30]. Second, two transgenic PkA1H1 lines, *Pv*DBP^{OR} in which the PkDBPα gene had been replaced with the *Pv*DBP gene (this transgenic insert was the full-length *Pv*DBP Salvador I (SalI) strain vaccine-homologous sequence), and *Pv*DBP^{OR}/Δβγ in which the same gene swap had taken place and additionally the native PkDBPβ and PkDBPγ genes had been deleted. This *Pv*DBP^{OR}/Δβγ line was considered the best model for *Plasmodium vivax* as the only DBP gene present in the parasite was the *Pv*DBP gene. Finally, there were also two transgenic control lines, PkDBPα^{OR} and PkDBPα^{OR}/Δβγ in which the native PkDBP genes had been deleted and replaced with re-codonised versions of themselves.

Only one of the anti-*Pv*DBPII mAbs, DB7, at high concentration, inhibited growth of the three *P. knowlesi* control lines (**Figure 3A**), suggesting an epitope cross-reactive with PkDBPα. In contrast, when assayed against the transgenic *Pv*DBP-expressing *Plasmodium knowlesi* lines, three of the mAbs showed high levels of inhibition of parasite growth, with four showing intermediate levels and the remaining three showing modest activity; whilst a control human mAb against *Ebolavirus*

showed no detectable GIA (**Figure 3A**). The three most neutralising anti-*Pv*DBPII mAbs in this assay (DB1, DB9 and DB10) had EC_{50} values comparable to mouse-derived mAbs which potently prevent erythrocyte invasion by *Plasmodium falciparum* [34, 35]. A strong correlation (P = 0.002, ρ=-0.951) was also observed between the association-rate (k_{on}) of the mAbs and GIA (**Figure 3B**), indicating that the opportunity for *Pv*DBP blockade in the context of merozoite invasion is likely to be time-limited [35, 36]. In contrast, this panel of mAbs showed no correlation between GIA and either dissociation rate or affinity (**Figure 3B**).

In addition, we tested the mAbs directly for their capacity to prevent reticulocyte invasion by *Plasmodium vivax* parasites derived from thirteen clinical isolates originating from Thai patients, using *ex-vivo* short-term culture invasion inhibition assays (**Figure 4A**). Sequencing of the *Pv*DBPII gene region from eight of these isolates revealed significant polymorphism (**Figure 4C**). Some isolates had *Pv*DBPII sequences identical to the SalI reference strain used in the vaccine (#4 and #7) while others were very polymorphic, with as many as ten amino acid substitutions in region II of the DBP gene (#6 and #8).

These assays revealed marked strain-dependent differences in the potency of the anti-*Pv*DBPII mAbs. For example, DB1 and DB10, the two most inhibitory mAbs in the transgenic *Plasmodium knowlesi* GIA assay (containing the SalI *Pv*DBP transgene), inhibited invasion of the Thai isolates with the same SalI *Pv*DBPII sequences (isolates #4 and #7) but not those with heterologous *Pv*DBPII sequences (isolates #5 and #8) (**Figure 4B,D**). Notably, for these two *Plasmodium vivax* parasite isolates which possessed the homologous SalI *Pv*DBPII sequence, the hierarchy of mAb potency also mirrored that observed in the transgenic *Plasmodium knowlesi* model (**Figure 4B**), suggesting this model is highly predictive of *P. vivax* neutralisation. Indeed, irrespective of some strain-dependence, mAbs DB3, 5, 6 and 7 showed intermediate median levels of inhibition (~40-60 %), whilst mAbs DB2, 4 and 8 showed low median levels (~10-20 %). However, in contrast to these data, only one of the

ten mAbs (DB9) potently inhibited invasion (~65-90 %) of 10/11 of the isolates against which it was tested. DB9 had also shown potent growth inhibition in the transgenic *P. knowlesi* assays of GIA (**Figure 3A**) and inhibited binding of all 5 variant alleles of *Pv*DBPII to DARC (**Figure 2B**), highlighting it as an antibody with broadly neutralising activity against a wide range of *P. vivax* variants.

Antagonism of DB9-mediated inhibitory activity

Having identified DB9 as a broadly neutralising mAb, we sought to assess whether its parasite-neutralising effects would be enhanced or diminished by combining it with the other nine mAbs in the panel. The BLI binding-competition assay (**Figure 1E-G**), showed that half of the mAbs, including DB9, compete with each other for binding sites on recombinant *Pv*DBPII. To test for evidence of synergy or antagonism [37] between DB9 and the other mAbs, we ran GIA assays using the *Pv*DBP^{OR} line of transgenic *P. knowlesi* in which DB9 was added at a fixed concentration of 25 µg/mL, together with a dilution series of one of the other nine mAbs (**Figure 5**). While no synergy was detected, there was apparent antagonism between DB9 and five of the other mAbs. Surprisingly, these were the five mAbs (DB1, DB4, DB5, DB7 and DB10) which did not compete with DB9 for binding to *Pv*DBPII in the BLI competition assay (**Figure 1E-G**). In contrast, the other four mAbs (DB2, DB3, DB6 and DB8), which bound epitopes overlapping with that of DB9, showed an additive growth inhibitory effect with DB9 in this assay. These data suggest that antibodies that bind in and around the DB9 epitope are able to function in an independent and additive manner, whilst antibodies that bind to distinct epitope regions elsewhere on the *Pv*DBPII molecule actively inhibit each other's functional activity. Given DB9 was able to show strain-transcending high-level neutralising activity, this raised the imperative to understand the epitope of DB9 and thus enable the future design of immunogens which specifically induce DB9-like antibodies.

The molecular basis for the action of DB9

To determine how DB9 binds to *Pv*DBPII, we produced a construct containing residues 211-508 of *Pv*DBPII by refolding material expressed in *E. coli*. This was mixed with Fab fragments of DB9 and the complex was crystallised. Crystals diffracted to 3.0 Å resolution, allowing structure determination by molecular replacement (**Figure 6** and **Table S3**). A comparison of the structure of *Pv*DBPII in complex with DB9 with that of un-liganded *Pv*DBPII revealed no change in *Pv*DBPII conformation (with an RMSD of 0.523Å).

The epitope of DB9 is contained solely within subdomain 3 of *Pv*DBPII (**Figure 6A**). This region consists of two long α-helices (H1 and H2), which form a platform on which three small helices (H3-H5) and their intervening loops are arranged (**Figure S2**). All three CDR loops of the heavy chain and CDR1 and CDR2 of the light chain directly contact *Pv*DBPII (**Figure S2** and **Table S4**). The epitope includes a single residue from H1 (K412) of *Pv*DBPII and residues from each of helices H3, H4 and H5, as well as the loops that link these helices. The contacts are predominantly mediated by hydrogen bonds between DB9 and hydrophilic residues from *Pv*DBPII.

In light of the broadly inhibitory potential of DB9, we next compared the position of the epitope with the locations of known polymorphic residues on *Pv*DBPII. The protein is known to be polymorphic with an alignment of globally disparate sequences of *Pv*DBPII finding over 120 polymorphic sites with nucleotide diversity varying between 0.006 and 0.0109 [38]. We retrieved 383 amino acid sequences of *Pv*DBPII and calculated their sequence entropies. This revealed that the surface of *Pv*DBPII contacted by DB9 is one of the most conserved regions of the domain, with low sequence variation, explaining its broadly reactive nature (**Figure 6B** and **Figure S2**).

In the membrane context *Pv*DBPII is thought to form a dimer, which can then interact with the extracellular domains of DARC. A crystal structure is available for a dimer of *Pv*DBPII bound to a

small helix, consisting of residues 19-30 of the extracellular ectodomain of DARC [15]. We next superimposed our *Pv*DBPII:DB9 structure onto this structure. This suggests a potential model for how DB9 might inhibit invasion by *P. vivax* (**Figure 6C**). While DB9 binds at a distance from the known region of the DARC binding site, it protrudes from subdomain 3 in the same direction as the C-terminus of the $DARC_{19-30}$ peptide. This end of the DARC peptide will face the transmembrane region of DARC, located in the reticulocyte membrane. Although the arrangement of $DARC_{31-60}$ is currently unknown, this model suggests that DB9 prevents the *Pv*DBPII dimer from approaching the reticulocyte membrane in an orientation which is compatible with DARC binding, thereby preventing initiation of the invasion process.

With the epitope for DB9 contained solely within subdomain 3, we next assessed the degree to which the other mAbs bind to this region. Subdomain 3 was produced by refolding material expressed in *E. coli*. An ELISA-based binding assay showed that 6 of the 10 mAbs bound subdomain 3 (**Figure S3**). With the exception of DB4, the mAbs that bind subdomain 3 were those that competed for binding on *Pv*DBPII (**Figure 1C**). Also interesting to note is that, with the exception of DB4, the mAbs that bind to subdomain 3 are not those that antagonise the effect of DB9. Therefore, despite the fact that antibodies that target subdomain 3 differ in their inhibitory potential, these data identify subdomain 3 of *Pv*DBPII as a promising potential target for broadly inhibitory antibodies, and identify the epitope of one such antibody.

DISCUSSION

The Duffy-binding protein is the most promising candidate for inclusion in a vaccine to prevent *P. vivax* due to its essential interaction with human DARC during reticulocyte invasion. While it has been shown that antibodies which bind to *Pv*DBP are found in individuals from malaria endemic regions, and their presence associates with protection from clinical vivax malaria [23-25], no human monoclonal antibody has been reported which targets *Pv*DBP and displays broadly inhibitory potential. We have therefore used vaccination of human volunteers with *Pv*DBPII to induce a humoral response and have isolated a monoclonal antibody which can inhibit all tested isolates of *P. vivax* from invading blood cells in a functional anti-parasitic assay. This monoclonal antibody has the potential to be used directly as a prophylactic to prevent vivax malaria and its epitope provides insight to guide future vaccine development.

The panel of mAbs generated in this study has been analysed through a series of complementary approaches and the differing outcomes of these assays illustrate the need for caution in attributing broadly inhibitory potential. The most accessible assay involves an analysis of purified protein binding in an ELISA-based format, with test antibodies assessed for their ability to prevent recombinant *Pv*DBPII from binding to the N-terminal DARC ectodomain, with the assumption that direct prevention of DARC binding is the goal for a protective antibody. This assay allows for the use of *Pv*DBPII variants to assess the breadth of inhibitory potential and identified two antibodies that broadly inhibited DARC binding (DB9 and DB2), and three with vaccine-homologous (SalI sequence) binding-inhibition activity (DB5, DB6 and DB7).

With the blood-stage of *P. vivax* still proving impossible to sustain in long-term *in vitro* culture conditions, this study also made the first use of a novel, culture-compatible transgenic parasite-based assay using the closely related simian malaria, *P. knowlesi*. Here the Duffy-binding protein, *Pk*DBPα was replaced by *Pv*DBP, generating novel parasite lines in which human RBC invasion

283 inhibition can be studied in a laboratory setting using long-term culture. This assay showed a clear
284 hierarchy of mAb potency against the transgenic parasites *in vitro*, and showed similar results for
285 parasites where the *Pk*DBPβ and *Pk*DBPγ genes had also been removed. Only one mAb (DB7)
286 showed modest cross-reactive GIA against the wild-type *P. knowlesi* strain. Most informatively, the
287 outcomes of this study only partially overlapped with those of the protein-based study, with some
288 antibodies (i.e. DB1 and DB10) among those with the greatest potency to block parasite invasion and
289 yet proving ineffective at blocking the *Pv*DBPII-DARC interaction in a protein-protein assay.
290
291 Finally, we used the most authentic *in vitro* assay available, by assessing the invasion of reticulocytes
292 by *ex-vivo P. vivax*, taken directly from patient isolates. When studying parasite isolates which
293 expressed the SalI *Pv*DBPII variant (matching that used in the transgenic *P. knowlesi* assays), these
294 studies give a very similar outcome to the transgenic *P. knowlesi* assays (Figures 3A and 4B).
295 However, when studying isolates with heterologous *Pv*DBPII sequences, the outcomes are different.
296 Here, one particular antibody, DB9, outperformed all of the rest in its capacity to inhibit reticulocyte
297 invasion by all tested strains. A comparison of data from these three assays suggests that use of
298 protein-protein analysis will miss valuable inhibitory antibodies and highlights the applicability of a
299 transgenic *P. knowlesi*-based assay as an accessible *in vitro* proxy for the *ex-vivo* analysis of *P. vivax*.
300 Future studies will use a panel of such transgenic parasites, engineered to express different *Pv*DBPII
301 variants, to allow the assessment of broadly-inhibitory potential of future vaccine approaches.
302
303 A variety of properties have been suggested as desirable for inhibitory antibodies that target *Pv*DBP,
304 including direct steric block of the DARC binding site or inhibition of dimerization [6, 13]. In contrast
305 to these, DB9 binds distantly from either the DARC-binding or dimerisation interfaces, on a non-
306 polymorphic site on the distal surface of subdomain 3. Remarkably, when DB9 binds to this surface,
307 it also prevents recombinant *Pv*DBPII from binding to DARC that is immobilised onto an ELISA plate.
308 A composite model, in which the structure of DB9 is docked onto the structure of a dimer of *Pv*DBPII

bound to the 19-30 peptide from DARC shows that DB9 emerges from the same side of *Pv*DBPII as the C-terminus of the DARC peptide. This suggests that it may sterically prevent dimeric *Pv*DBPII from approaching a DARC coated surface, either on an ELISA plate or a reticulocyte membrane, and thereby prevent receptor engagement and invasion.

These findings have significant consequences for vaccine development, identifying subdomain 3 of *Pv*DBPII as an important region for the presentation of broadly-inhibitory epitopes for human antibodies. Not all of the antibodies identified to bind to subdomain 3 are inhibitory. However, our discovery of a set of antibodies which bind to *Pv*DBPII and antagonise the function of the broadly inhibitory DB9 also raises the imperative for future vaccine design to avoid inducing these deleterious antibodies. It is therefore encouraging to note that 80% of the antibodies that antagonise the function of DB9 do not recognise subdomain 3. This suggests future vaccination strategies in which the surface of subdomain 3 containing the DB9 epitope is specifically presented to the immune system in the form of a vaccine immunogen. Such an approach has the potential to generate the malaria vaccines of the future.

ACKNOWLEDGEMENTS

The authors are grateful for the assistance of Julie Furze, David Llewellyn, Drew Worth (Jenner Institute, University of Oxford); Patrick C. Wilson (University of Chicago) for providing mAb expression plasmids; Oleg Fedorov (Structural Genomics Consortium, University of Oxford) for the use of the Octet RED384 machine; Amy Duckett and Carly Banner (University of Oxford) for arranging contracts; Yves Durocher for provision of HEK293E cells (CNRC-NRC, Canada); A. Rushdi Shakri (ICGEB, India) and Chetan E. Chitnis (Institute Pasteur) for provision of *Pv*DBPII variant proteins used in the binding inhibition assays; Olivier Bertrand (INSERM, Paris) for the VHH camelid anti-DARC nanobody; and all the VAC051 *Pv*DBPII vaccine clinical trial study volunteers.

This work was supported in-part by funding from the European Union's Horizon 2020 research and innovation programme under grant agreement for MultiViVax [number 733073]. T.A.R. held a Wellcome Trust Research Training Fellowship [108734/Z/15/Z]; N.M.B. is funded by a Wellcome Trust D. Phil. program in Structural Cell Biology; D.G.W.A. held a UK MRC iCASE PhD Studentship [MR/K017632/1]; M.K.H. is a Wellcome Trust Senior Investigator [101020/Z/13/Z]; and S.J.D. is a Jenner Investigator; a Lister Institute Research Prize Fellow and a Wellcome Trust Senior Fellow [106917/Z/15/Z]. R.W.M and F.M are supported by an MRC Career Development Award (MR/M021157/1) 603 jointly funded by the UK Medical Research Council and Department for International Development.

AUTHOR CONTRIBUTIONS

T.A.R, N.M.B, M.K.H. and S.J.D. conceived the study and wrote the manuscript.

T.A.R, N.M.B, M.K.H., F.M., J.S.C., V.K., S.G., D.G.W.A., G.M.L., S.C.E, S.E.S., D.Q., J.J., J.M.M., R.W.M. and M.K.H. performed experiments.

T.A.R, N.M.B., F.M., J.S.C., D.G.W.A., M.K.H. and S.J.D. performed data analysis and interpretation.

J.J., R.W.M., B.R., L.R. and F.H.N. contributed reagents or materials and facilities.

DECLARATION OF INTERESTS

D.G.W.A, M.K.H. and S.J.D. are named inventors on patent applications relating to malaria vaccines, mAbs and/or immunization regimens.

METHODS

Generation of monoclonal antibodies

Plasmablast isolation and sorting: Volunteers from a Phase Ia clinical trial were bled seven days after the second immunisation using MVA (modified vaccinia virus Ankara) encoding *Pv*DBPII [19]. Blood was collected from volunteers in heparinised tubes and centrifuged in Leucosep tubes (Greiner Bio-One) to separate the peripheral blood mononuclear cells (PBMC). The PBMC were enriched for B cells using a human pan-B cell enrichment kit (Easysep) and re-suspended in DMEM before staining with a $CD19^{+}$, $CD10^{-}$, $CD21^{-}$, $CD27^{+}$, $CD20^{-}$, $CD38^{+}$, IgG^{+} fluorophore-conjugated antibody panel. Plasmablasts were single-cell sorted using a MoFlo cell sorter (DakoCytomation) into 96-well PCR plates containing 10 µL 10 mM Tris HCl buffer containing 40 U/mL of RNase inhibitor (Promega). The study received ethical approval from the Oxfordshire Research Ethics Committee A in the UK (REC reference 13/SC/0001). The volunteers signed consent forms and consent was verified before each vaccination.

Antibody variable gene amplification: In wells of a 96-well plate, each containing a single antibody-secreting cell (ASC), a two-step RT-PCR was carried out with a first reverse transcription (RT) step using a Sensiscript RT kit (Qiagen) and degenerate primers 1-17 (modified from [39], see **Supplemental Experimental Procedures Table 1**). Next, a PCR was performed on 1 µL of the RT reaction product using the same set of primers used before (1-17) which cover the diversity of all Vγ, Vκ and Vλ sequences using Phusion HF master mix (New England Biolabs). Following this, a nested PCR was performed with primers 18-51, also using Phusion HF master mix, (**Supplemental Experimental Procedures Table 1**) on 1 µL of the previous product diluted 1:100 to amplify inserts which contain plasmid-homologous extensions designed for circular polymerase extension cloning [40].

Cloning: The AbVec-hIgG1/AbVec-hIgKappa/AbVec-hIgLambda expression plasmids were a kind gift from Patrick C. Wilson (University of Chicago) [41]. These plasmids were 5' digested using BshTI and at the 3' using SalI (AbVec-hIgG1), XhoI (AbVec-hIgLambda) and Pfl23II (AbVec-hIgKappa) to yield linear products. CPEC assembly was performed by mixing 100 ng of a 1:1 molar ratio of insert:plasmid in 20 µL containing 1x Phusion HF polymerase master mix and assembled using an 8-cycle CPEC protocol (8 cycles: 98 ˚C 10 s, slow ramp anneal 70 ˚C ➔ 55 ˚C at 0.1 ˚C/s, 72 ˚C 35 s). Full nicked plasmids were then transformed into Zymo 5α Mix & go competent *Escherichia coli* (Zymo Research) according to manufacturer's instructions, streaked on LB agar petri dishes containing 100 µg/mL carbenicillin and grown at 37°C overnight in a static incubator. Colonies were screened by PCR for correctly sized inserts.

Screening: Exponential growth-phase adherent HEK293 cells were re-suspended in DMEM (Sigma-Aldrich) supplemented with 2 mM L-glutamine, 100 U/mL penicillin, 1 mM sodium pyruvate, 0.1 mg/mL streptomycin and 10 % ultra-low IgG foetal bovine serum (FBS) (Thermo Fischer Scientific) and seeded at 4 x 10^4 cells/well in 100 µL 24 h prior to transfection in Costar 96-well cell culture plates (Corning). On the day of transfection, for each well, 50 µL of 60 µg/mL linear 25 kDa PEI (Alfa Aesar) was mixed with 200 ng of cognate heavy- and light-chain coding plasmid in a volume of 50 µL and shaken at 20°C for 30 min. The DNA-PEI complexes were added to the HEK293 cells. The following day, an additional 50 µL of supplemented DMEM (as described above) was added to each well. Supernatants were screened for *Pv*DBPII (produced in S2 cells as described below) binding by indirect ELISA.

Recombinant protein constructs, expression and purification

The production of the recombinant *Pv*DBPII used in the IgG screening assay described above, the DARC-binding inhibition assays (**Figure 2**) and the SPR assays (**Figure 1A-D**), from *Drosophila* S2 cells has been previously described [19]. In brief; the sequence used was identical to the vaccine

sequence; D194–T521 of *Pv*DBPII (SalI), with T257A, S353A and T422A substitutions to remove sites of possible N-linked glycosylation, followed by a shortened Pk/V5 epitope tag (IPNPLLGLD) and a C-tag (EPEA) [42] for detection and purification, respectively. Purification was performed on an AKTA Pure 25 system (GE Healthcare, UK), consisting of an affinity step with CaptureSelect™ C-tag column (Thermo Fisher Scientific, UK) and a polishing size exclusion chromatography (SEC) using Superdex 200 16/60 PG (GE Healthcare, UK) in 20 mM Tris-HCl, 150 mM NaCl, pH 7.4 (TBS). Purified protein was quantified by Nanodrop (Thermo Fisher Scientific, UK) and stored at -80°C until further use. A gene encoding the *Pv*DBPII HMP013 allele [19] (aa 194-521) was codon optimised for human expression and synthesised (Genewiz, USA). This sequence, with a 5' KpnI site and 3' XbaI site, was cloned into a mammalian expression plasmid in frame with an N-terminal mouse IgK light chain leader sequence and a C-terminal C-tag prior to the stop codon. Suspension EXPI293F cells (Thermo Fisher Scientific, UK) were transiently transfected and culture supernatants were harvested after 4 days. Purification was performed on an AKTA Pure 25 system (GE Healthcare, UK), consisting of an affinity step with CaptureSelect™ C-tag column (Thermo Fisher Scientific, UK) and a polishing SEC step using Superdex 200 Increase 10/300 GL (GE Healthcare, UK) in 20 mM Tris-HCl, 150 mM NaCl, 0.1% Tween 20, pH 7.4 (TBS). Purified protein was quantified by Nanodrop (Thermo Fisher Scientific, UK) and stored at -80°C until further use.

The *Pv*AH, *Pv*O and *Pv*P alleles of PvDBPII [43] used in the DARC binding-inhibition assays (**Figure 2**) were a kind gift from Chetan Chitnis.

Monobiotinylated *Pv*DBPII supernatant was produced for use in the BLI experiments (**Figures 1E-G**) by transient transfection of suspension EXPI293F cells, using a plasmid encoding *Pv*DBPII (SalI) with C-terminal rat CD4 domains 3 and 4 followed by a biotin acceptor peptide obtained from Addgene (plasmid #68529) and courtesy of Dr Julian Rayner (Wellcome Trust Sanger Institute, Hinxton, UK) [44]. This *Pv*DBPII plasmid was co-transfected with another plasmid encoding *E. coli* biotin ligase (BirA). Supernatant was harvested after 4 days, clarified, dialysed against PBS using snakeskin and concentrated ~10-fold using spin columns.

The production of the *Pv*DBPII and *Pv*DBPII subdomain 3 proteins used in the crystal complex (Figure 6) and the subdomain 3 binding ELISA (Figure S3) is described in 'Structural Methods' below.

The production of recombinant N-terminal DARC, used in the DARC-binding inhibition assays, has been previously described [19]. In brief; a gene encoding the first 60 amino acids of DARC Fyb allele (GenBank Accession #ABA10433.1) followed by a thrombin cleavage site (LVPRGS) and an AviTag (GLNDIFEAQKIEWHE) was codon-optimised for *E. coli* expression and synthesised (GeneArt, Life Technologies). Cysteines 4, 51 and 54 of DARC were mutated to alanine. This sequence with 5' KpnI site and 3' BamHI site was cloned into a mammalian expression plasmid in-frame with an N-terminal human tissue plasminogen activator (tPA) leader sequence [20] and a C-terminal hexa-histidine (His6) tag prior to the stop codon. Suspension HEK293E cells grown in EXPI293 expression medium (Thermo Fisher Scientific, UK) were transiently transfected with plasmid and allowed to grow for three days before the supernatant was harvested, purified using a HisTrap Excel column (GE Healthcare, UK) and buffer exchanged into PBS. Purified protein was quantified by Nanodrop (Thermo Fisher Scientific, UK) and stored at -80°C until further use.

Recombinant monoclonal antibodies were transiently expressed in HEK293F cells using the Expi293™ *Expression* System (Thermo Fischer Scientific) according to the manufacturer's recommendations. Cognate heavy and light chain-coding plasmids were co-transfected at a 1:1 ratio. Supernatants were harvested by centrifuging the culture at 2500 x*g* for 15 min and filtering the supernatant with a 0.22 µm vacuum filter. All mAbs were purified using a 5 mL Protein G HP column (GE Healthcare) on an ÄKTA start FPLC system or an ÄKTA Pure FPLC system (both GE Healthcare). Equilibration and wash steps were performed with Dulbecco's PBS and mAbs were eluted in 0.1 M glycine pH 2.7. The eluates were pH equilibrated to 7.4 using 1.0 M Tris HCl pH 9.0 and immediately buffer-exchanged into Dulbecco's PBS and concentrated using an Amicon® ultra centrifugal concentrator (Millipore) with a molecular weight cut-off of 30 kDa.

Bio-Layer Interferometry (BLI)

BLI was carried out on an OctetRED384 (Pall FortéBio) using streptavidin-coated biosensors (Pall FortéBio) to immobilise *Pv*DBPII enzymatically monobiotinylated on a C-terminal AviTag™. Assays were carried out in 96-well format in black plates (Greiner). For epitope binning studies (**Figure 1E-G**), a six-step sequential assay was performed: Baseline (PBS, 30 s); Protein immobilisation (neat supernatant, 120 s); Wash (PBS, 60 s); first mAb (mAb1) binding (300 nM mAb1, 120 s); Wash (PBS, 60 s); second mAb (mAb2) binding (150 nM mAb2, 120 s). "Relative binding" in **Figure 1E** shows the ratio ($Signal_{mAb2}$ with mAb1 bound)/($Signal_{mAb2}$ with no mAb1) where "$Signal_{mAb2}$" was normalised for the amount of *Pv*DBPII bound to the biosensor, such that "$Signal_{mAb2}$" = the raw signal in "mAb2 binding" divided by the raw signal in the "Protein immobilisation" phase. The resulting "binding profile" for any given mAb corresponds to the column of "relative binding values" under that mAb in the "relative binding" table. To establish the epitope bins, binding profiles between each mAb pair were correlated using a Pearson product-moment correlation coefficient, the values of which are shown in the "binding profile correlation" matrix in **Figure 1F**. mAb pairs whose binding profile correlation was > 0.7 were grouped into the same epitope bin (**Figure 1G**).

Measurement of binding by ELISA

Qualitative mAb binding ELISAs such as those used in **Figure S3** were carried out by coating *Pv*DBPII or *Pv*DBPII subdomain 3, produced as described in 'Structural Methods' above, on Maxisorp flat-bottom 96-well ELISA plates (Nunc) at 2 µg/mL in 50 µL at 4 °C overnight. Plates were then washed twice with PBS and 0.05% Tween 20 (PBS/T) and blocked with 200 µL of Blocker™ Casein (Thermo Fischer Scientific) for 1 h. Next, wells were incubated with 1000 ng/mL of mAb for approximately 45 min at 20 °C then washed 4 times with PBS/T before the addition of 50 µL of goat anti-human gamma-chain alkaline phosphatase-conjugated secondary antibody (Sigma-Aldrich) for 45 min at 20 °C. Wells were then washed 6 times with PBS/T and developed with 100 µL of p-nitrophenyl

484 phosphate substrate at 1 mg/mL (Sigma-Aldrich) and optical density read at 405 nm (OD_{405}) using a
485 Model 550 Microplate Reader (Bio-Rad, UK).
486
487 **Affinity determination by SPR**
488 Data were collected on a Biacore X100 (GE Healthcare). Experiments were performed at 25 °C in
489 Dulbecco's PBS + 0.005 % Polysorbate-20 (GE Healthcare). In **Figure 1** and **Table S2** a sensor chip
490 protein A (GE Healthcare) was used to capture 50-100 RU of purified mAb diluted in SPR running
491 buffer at a flow rate of 5 µL/min on flow cell 2. Next, an appropriate range (typically 20 nM-0.625
492 nM) of six 2-fold dilutions, with one replicate, of *Pv*DBPII (expressed in S2 cells as described above)
493 was injected for 90 s at 60 µL/min and dissociation was measured for 1600 s (7200 s when
494 necessary). Specific binding of the *Pv*DBPII protein to mAb was obtained by reference-subtracting
495 the response of a blank surface from that of the mAb-coated surface. The sensor surface was
496 regenerated with a 60 s pulse of 10 mM glycine-HCl pH 1.5 (GE Healthcare). Sensorgrams were fitted
497 to a global Langmuir 1:1 interaction model, allowing determination of the kinetic association and
498 dissociation rate constants using Biacore X100 evaluation software.
499
500 ***Pv*DBPII-DARC binding inhibition assays**
501 This assay methodology has been previously reported [19, 29]. In brief; recombinant N-terminal
502 DARC protein was coated onto Nunc-Immuno Maxisorp plates at 1 µg/mL. mAb samples were
503 diluted down in a 2-fold series (starting at 100 µg/mL) and pre-incubated with *Pv*DBPII protein for 30
504 min at room temperature (RT). The pre-incubated *Pv*DBPII protein plus mAb mixture was then added
505 to the DARC-coated plates (in duplicate wells). The plates were incubated for 1 h at 37 °C, washed
506 and then incubated with anti-*Pv*DBPII polyclonal rabbit serum [20]. After a further wash step, the
507 plates were incubated with a 1:1000 dilution of anti-rabbit IgG alkaline phosphatase (Sigma Aldrich,
508 UK) and then developed with 1 mg/mL p-nitrophenyl phosphate in diethanolamine buffer (Pierce,
509 UK). OD_{405} was read using a Model 550 Microplate Reader (Bio-Rad, UK) when control wells

containing *Pv*DBPII protein and buffer only reached a value of 1.0. In one column of each 96 well plate, wells contained only mAb (100 µg /ml) and buffer (no *Pv*DBPII protein) and these 'background' OD_{405} values were subtracted from all test values. To calculate % binding-inhibition for each mAb sample the formula below was used:

1 – (OD_{405} value of mAb sample / OD_{405} value of negative control sample) x 100

Five allelic variants of recombinant *Pv*DBPII were used in the assay; Sal1, which was made in S2 cells as described above; *Pv*AH, *Pv*O and *Pv*P alleles [43], which were a kind gift from Chetan Chitnis; and *Pv*HMP013, which was sequenced from a vivax-infected patient in Australia [45]. The expression of recombinant *Pv*DBPII HMP013 protein has been previously described [19] and is summarised above. An anti-*Ebolavirus* glycoprotein-reactive human IgG1 mAb 'EBL040' (Rijal P *et al.*, submitted) was used as a negative isotype control for mAb samples. Polyclonal human anti-*Pv*DBPII serum from the clinical trial [19] was used as the positive control.

Genetic modification of *P. knowlesi* parasites

The genetic modification of *P. knowlesi* A1H1 strain [30] is described in detail elsewhere (Mohring F *et al*., manuscript under). Briefly, parasites were modified using a two-plasmid CRISPR-Cas9 system, comprised of a plasmid (pCas/sg) providing Cas9, sgRNA, and a hDHFR-yFCU (for positive and negative selection) to create a locus specific double strand break and a separate "donor" DNA plasmid (pDonor) to act as the repair template. To create the $PkDBP\alpha^{OR}$ or $PvDBP^{OR}$ lines the PkDBPα locus (sgRNA: GCTGATCCAGGTTCTCAATC) was targeted using a pDonor plasmid containing full length recodonised PkDBPα or PvDBP (SalI) genes respectively, both flanked by 500 bp homology regions targetting the 5'UTR and 3'UTR of PkDBPα. To create the *Pk*$DBP\alpha^{OR}$/Δβγ and *Pv*DBP^{OR}/Δβγ lines this process was repeated in an A1-H.1 line which had a natural deletion of DBPβ (truncation of chromosome 14) and then a subsequent round of gene editing used to delete the DBPγ locus (sgRNA: CATGCAACAATTTACACCCC) using a pDonor plasmid containing a spacer sequence flanked by 500 bp homology regions targetting the 5'UTR and 3'UTR of PkDBPγ.

536

537 **Assays of growth inhibitory activity (GIA) with *P. knowlesi* lines**

538 ***In vitro* parasite culture and synchronisation.** Human RBC-adapted parasites were maintained in
539 culture as previously described [30]. Briefly, parasites were grown at 2 % haematocrit in O+ human
540 RBC, which were prepared twice monthly. Culture medium contained 10 % heat-inactivated pooled
541 human serum mixed with RPMI 1640 supplemented with 25 mM HEPES, 35 µM hypoxanthine, 2 mM
542 L-glutamine and 20 µg/mL gentamycin. Parasite cultures were synchronised at trophozoite/schizont
543 stage by magnetic separation (MACS LS columns, Miltenyi Biotech).

544 ***In vitro* assay of GIA.** Methodology was adapted from the protocol of the International GIA
545 Reference Centre at NIH, USA [46]. Synchronised trophozoites were adjusted to 1.5 % parasitaemia,
546 and 20 µL aliquots were pipetted into 96-well flat/half area tissue culture cluster plates (Appleton
547 Woods). 20 µL test antibody or controls were added in duplicate or triplicate test wells over a
548 concentration range (usually; 1, 0.5, 0.25, 0.125, 0.0625, 0.0312, 0.015 and 0.0075 mg/mL) and
549 incubated for one erythrocytic parasite cycle (26-30 h). Parasitaemia was measured using the lactate
550 dehydrogenase (pLDH) activity assay following standard protocols [47]. Percentage GIA was
551 calculated as below;

552 **% GIA = 100 – 100 (Sample A_{650} – Uninfected RBC A_{650})/(Infected ControlA_{650} – Uninfected RBC A_{650})**

553 An anti-DARC VHH camelid nanobody [48], a kind gift from Dr Olivier Bertrand (INSERM, France) was
554 included in the test plate as a positive control in every assay (at a final concentration of 6, 3 or 1.5
555 µg/mL) and an anti-*Ebolavirus* glycoprotein-reactive human IgG1 mAb as a negative isotype control
556 for mAb samples. The assays were performed using five different lines of *P. knowlesi* parasites; the
557 non-transgenic strain (PkA1H1); two transgenic lines containing the *Pv*DBP gene (*Pv*DBP^{OR} and
558 *Pv*DBP^{OR}/Δβγ) and two transgenic control lines (PkDBPα^{OR} and PkDBPα^{OR}/Δβγ) (Mohring F *et al.*,
559 submitted). In the mAb synergy assays (**Figure 5**) 'Bliss additivity' between two mAbs (mAb A and
560 mAb B) was calculated using the formula below.

561 $$\mathbf{GIA\ [A+B]\ Bliss} = \left[1 - \left(1 - \frac{\mathbf{GIA\ A}}{100}\right) * \left(1 - \frac{\mathbf{GIA\ B}}{100}\right)\right] * 100$$

562

563 ***Ex-vivo P. vivax* invasion assays**

564 The assay methodology has been previously described [49, 50]. The major steps are summarised
565 below.

566 **Purification of reticulocytes from umbilical cord blood:** 20 mL aliquots of umbilical cord blood were
567 collected from consenting volunteers (OXTREC 027-025 (Center for Clinical Vaccinology and Tropical
568 Medicine, University of Oxford, Oxford, United Kingdom) and MUTM 2008-215 from the Ethics
569 Committee of the Faculty of Tropical Medicine (Mahidol University, Bangkok, Thailand)) in lithium
570 heparin tubes and the white blood cells and platelets depleted using Non-woven filters™ (Antoshin).
571 The RBC were then layered onto 70 % isotonic Percoll, centrifuged and the resulting band of
572 enriched reticulocytes was incubated with anti-CD71 MicroBeads (Miltenyi) before being passed
573 through a large selection (LS) column (Miltenyi) to obtain a CD71-depleted (negative) fraction and a
574 CD71-rich fraction (positive). The purity levels of these CD71+ fractions were assessed with
575 microscopy using new methylene blue staining (Sigma-Aldrich).

576 **Purification of schizonts from *ex-vivo P. vivax*-infected blood samples:** 5 mL samples of whole
577 blood were collected from consenting patients (OXTREC 027-025 (Center for Clinical
578 Vaccinology and Tropical Medicine, University of Oxford, Oxford, United Kingdom)
579 and MUTM 2008-215 from the Ethics Committee of the Faculty of Tropical Medicine
580 (Mahidol University, Bangkok, Thailand)) diagnosed with *P. vivax* malaria and rapidly transported at
581 RT back to the laboratory. Samples were not collected from patients who had taken antimalarial or
582 antimicrobial drugs within the previous month, or whose parasitaemia was < 0.1 % on smear
583 microscopy. The samples were leukodepleted using Non-woven filters™ (Antoshin), and the
584 parasites were cultured to schizont stage. The culture was then treated with trypsin, overlaid on a 45
585 % Percoll (isotonic) cushion and centrifuged to isolate a fine band of concentrated schizonts for use
586 in the assay.

Invasion assay: The concentrated schizont preparation was mixed with the enriched reticulocyte fraction at a ratio of 1:6, giving a starting schizont parasitaemia of ~14 %. The mixture was diluted to 1.3 % haematocrit in 300 µL of complete McCoy 5A medium and cultured in 96-well cell culture plates in an atmosphere of 5 % O_2 at 37.5 °C. Test antibodies and controls were buffer exchanged into *Pv* culture medium (McCoy 5A medium (Gibco) supplemented with 2.4 g/L D-glucose, 40 mg/mL gentamycin sulfate, and 20% heat-inactivated human AB serum) and added to the final invasion assay mixture at the desired concentration. In the case of the anti-*Pv*DBPII mAbs this was 1 mg/mL. The anti-DARC nanobody, at 25 µg/mL, and the recombinant IgG1 anti-*Ebolavirus* mAb, at 1mg/mL, were added to all assays as positive and negative controls respectively. Maturation was obtained after incubation for an average of 24 h. At the end of the incubation period, thin smears (each made with 1 µL packed cells) were made, and stained with Giemsa (Sigma-Aldrich). The number of ring stages and trophozoites per 4000 erythrocytes was determined by examining the Giemsa thin film smears by light microscopy. For isolates #1-3, the invasion assays were performed in Singapore using cryopreserved Thai *P.vivax* isolates and reticulocyte invasion inhibition was quantified by flow cytometry as previously described [49].

Sequencing of the *Pv*DBPII gene from Thai isolates: Genomic DNA was extracted either from an aliquot (200 µL) of the initial blood sample or from a dried blood spot, using the DNeasy Blood and Tissue kit (QIAGEN). PCR amplification was performed on 1 µL purified genomic DNA in a total volume of 50 µL, containing 1x PCR buffer, 2.5 mM $MgCl_2$, 0.2 mM of each dNTP, 2 µM each primer (forward 5' – gtg act ggg cat gag gga aat tct cg and reverse 5' – gcg tag aat ctc ctg gaa cct tct cc) and 1.25U of AmpliTaq Gold DNA polymerase (Applied Biosystems). The cycling conditions were: 95 °C for 5 min followed by 30 cycles at 94 °C for 1 min, 63 °C for 2 min, and 72 °C for 2 min. The product was purified using the QIAquick PCR purification kit (QIAGEN) and then sequenced (GATC biotech).

Structural Methods

Protein Cloning, Expression and Purification

*Pv*DBPII coding region (residues 211-507; SalI sequence) was cloned into pET15b vector. This vector allowed expression of the protein with an N-terminal His6 tag and a TEV cleavage site, in *E. coli* (BL21-DE3 strain). The transformed bacteria were induced with 1 mM IPTG at an optical density of 0.8 at 600 nm. *Pv*DBPII was expressed exclusively in inclusion bodies and was prepared as previously described [15]. In short, the inclusion bodies were solubilised in 6 M guanidine hydrochloride, 20 mM Tris pH8, 300 mM NaCl, and refolded by flash-dilution into 400 mM L-arginine, 50 mM Tris pH8, 10 mM EDTA, 0.1 mM PMSF, 3 mM reduced glutathione, and 0.3 mM oxidised glutathione. Refolded proteins were buffer exchanged into 20 mM Tris pH8, 150 mM NaCl, 20 mM imidazole and then affinity purified on NiNTA resin. The His-tag was removed by TEV protease cleavage and the tagless *Pv*DBPII was separated from the His-tag on NiNTA resin and purified by SEC (S75 16/60, GE Healthcare) into 20 mM Hepes pH7.5, 150 mM NaCl.

Subdomain3 (Sd3) (residues 211-508) was subcloned from the *Pv*DBPII construct in the pET15b vector. Sd3 also expressed in *E. coli* BL21 (DE3) cells in the insoluble fraction and was solubilised in 6 M guanidine hydrochloride, 20 mM Tris (pH8), 150 mM NaCl, 20 mM imidazole. Sd3 was then refolded by binding to a NiNTA column and gradually decreasing the concentration of guanidine hydrochloride, until the protein was in 20 mM Tris (pH8), 150 mM NaCl, 20 mM imidazole. The refolded Sd3 protein was then eluted and further purified using SEC (S75 16/60 GE Healthcare) into 20 mM Hepes pH7.5, 150 mM NaCl.

Fab Generation and Purification

Fab fragments for DB9 were generated from IgG by incubating with immobilised papain (ThermoFisher Scientific) for 16 h at 37 °C. The Fab was separated from the un-cleaved DB9 and Fc

637 regions using protein A resin (ThermoFisher Scientific). The Fab fragments were then purified by SEC
638 into 20 mM Hepes pH7.5, 150 mM NaCl.
639
640 **Protein Cystallisation and Data Collection**
641 *Pv*DBPII and DB9Fab were mixed in a 1.2:1 molar ratio and incubated at RT for 1 h. The complex was
642 purified by SEC (S75, GE Healthcare) in 20 mM Hepes pH7.5, 150 mM NaCl. Broad crystallisation
643 trials were set up by sitting-drop vapour diffusion in SwisSci 96-well plates by mixing 100 nl protein
644 with 100 nl reservoir solution. Crystals grew in the reservoir solution of 45 % v/v polypropylene
645 glycol 400, 10% v/v ethanol and were then cryo-cooled in liquid nitrogen. Data were collected on
646 beamline I03 at Diamond Light Source and were indexed and scaled using Scaler [51] to a resolution
647 of 3.04 Å.
648
649 **Structure Solution**
650 The *Pv*DBPII:DB9Fab structure was solved by molecular replacement in Phaser [52] using the known
651 structures of *Pv*DBPII (PDB 4NUV) and a human mAb Fab fragment (PDB: 3DIF), separated into two
652 files containing the variable and constant regions, as search models. This identified one copy of the
653 *Pv*DBPII:DB9 complex in the asymmetric unit. Refinement and rebuilding was completed using
654 Buster [53] and Coot [54], respectively.
655
656 **Statistical Analyses**
657 Data were analysed using GraphPad Prism version 6.07 for Windows (GraphPad Software Inc.). In
658 **Figures 3A**, a four-parameter sigmoidal dose-response curve was fitted to the relationship
659 between log10 (antibody concentration) and percentage GIA for each dataset and used to
660 interpolate EC_{30} values. In **Figure 3B**, the nonparametric Spearman's rank correlation coefficient
661 (ρ) was used to assess a correlation between the variables $K_{on}/K_{off}/K_D$ and GIA EC_{30}. In all
662 statistical tests the *P* values reported are two-tailed with $P < 0.05$ considered significant.

REFERENCES

1. WHO, *Control and elimination of plasmodium vivax malaria: a technical brief. ISBN 978 92 4 150924 4.* 2015.
2. Gething, P.W., et al., *A long neglected world malaria map: Plasmodium vivax endemicity in 2010.* PLoS Negl Trop Dis, 2012. **6**(9): p. e1814.
3. Gruszczyk, J., et al., *Transferrin receptor 1 is a reticulocyte-specific receptor for Plasmodium vivax.* Science, 2018. **359**(6371): p. 48-55.
4. Malleret, B., L. Renia, and B. Russell, *The unhealthy attraction of Plasmodium vivax to reticulocytes expressing transferrin receptor 1 (CD71).* Int J Parasitol, 2017. **47**(7): p. 379-383.
5. Singh, S.K., et al., *Structural basis for Duffy recognition by the malaria parasite Duffy-binding-like domain.* Nature, 2006. **439**(7077): p. 741-4.
6. Chitnis, C.E. and A. Sharma, *Targeting the Plasmodium vivax Duffy-binding protein.* Trends Parasitol, 2008. **24**(1): p. 29-34.
7. Singh, A.P., et al., *Targeted deletion of Plasmodium knowlesi Duffy binding protein confirms its role in junction formation during invasion.* Mol Microbiol, 2005. **55**(6): p. 1925-34.
8. Singh, A.P., S.K. Puri, and C.E. Chitnis, *Antibodies raised against receptor-binding domain of Plasmodium knowlesi Duffy binding protein inhibit erythrocyte invasion.* Mol Biochem Parasitol, 2002. **121**(1): p. 21-31.
9. Miller, L.H., et al., *The resistance factor to Plasmodium vivax in blacks. The Duffy-blood-group genotype, FyFy.* N Engl J Med, 1976. **295**(6): p. 302-4.
10. Howes, R.E., et al., *Plasmodium vivax Transmission in Africa.* PLoS Negl Trop Dis, 2015. **9**(11): p. e0004222.
11. Culleton, R.L., et al., *Failure to detect Plasmodium vivax in West and Central Africa by PCR species typing.* Malar J, 2008. **7**: p. 174.
12. Draper, S.J., et al., *Malaria Vaccines: Recent Advances and New Horizons.* Cell Host Microbe, 2018. **24**(1): p. 43-56.
13. Batchelor, J.D., J.A. Zahm, and N.H. Tolia, *Dimerization of Plasmodium vivax DBP is induced upon receptor binding and drives recognition of DARC.* Nat Struct Mol Biol, 2011. **18**(8): p. 908-14.
14. Choe, H., et al., *Sulphated tyrosines mediate association of chemokines and Plasmodium vivax Duffy binding protein with the Duffy antigen/receptor for chemokines (DARC).* Mol Microbiol, 2005. **55**(5): p. 1413-22.
15. Batchelor, J.D., et al., *Red blood cell invasion by Plasmodium vivax: structural basis for DBP engagement of DARC.* PLoS Pathog, 2014. **10**(1): p. e1003869.
16. Hans, D., et al., *Mapping binding residues in the Plasmodium vivax domain that binds Duffy antigen during red cell invasion.* Mol Microbiol, 2005. **55**(5): p. 1423-34.
17. VanBuskirk, K.M., E. Sevova, and J.H. Adams, *Conserved residues in the Plasmodium vivax Duffy-binding protein ligand domain are critical for erythrocyte receptor recognition.* Proc Natl Acad Sci U S A, 2004. **101**(44): p. 15754-9.
18. Singh, K., et al., *Malaria vaccine candidate based on Duffy-binding protein elicits strain transcending functional antibodies in a Phase I trial.* NPJ Vaccines, 2018. **3**: p. 48.
19. Payne, R.O., et al., *Human vaccination against Plasmodium vivax Duffy-binding protein induces strain-transcending antibodies.* JCI Insight, 2017. **2**(12).
20. de Cassan, S.C., et al., *Preclinical Assessment of Viral Vectored and Protein Vaccines Targeting the Duffy-Binding Protein Region II of Plasmodium Vivax.* Front Immunol, 2015. **6**: p. 348.
21. Moreno, A., et al., *Preclinical assessment of the receptor-binding domain of Plasmodium vivax Duffy-binding protein as a vaccine candidate in rhesus macaques.* Vaccine, 2008. **26**(34): p. 4338-44.

22. Bermudez, M., et al., *Plasmodium vivax in vitro continuous culture: the spoke in the wheel.* Malar J, 2018. **17**(1): p. 301.
23. Cole-Tobian, J.L., et al., *Strain-specific duffy binding protein antibodies correlate with protection against infection with homologous compared to heterologous plasmodium vivax strains in Papua New Guinean children.* Infect Immun, 2009. **77**(9): p. 4009-17.
24. King, C.L., et al., *Naturally acquired Duffy-binding protein-specific binding inhibitory antibodies confer protection from blood-stage Plasmodium vivax infection.* Proc Natl Acad Sci U S A, 2008. **105**(24): p. 8363-8.
25. Nicolete, V.C., et al., *Naturally Acquired Binding-Inhibitory Antibodies to Plasmodium vivax Duffy Binding Protein and Clinical Immunity to Malaria in Rural Amazonians.* J Infect Dis, 2016. **214**(10): p. 1539-1546.
26. Chen, E., et al., *Broadly neutralizing epitopes in the Plasmodium vivax vaccine candidate Duffy Binding Protein.* Proc Natl Acad Sci U S A, 2016. **113**(22): p. 6277-82.
27. Chootong, P., et al., *Mapping epitopes of the Plasmodium vivax Duffy binding protein with naturally acquired inhibitory antibodies.* Infect Immun, 2010. **78**(3): p. 1089-95.
28. Ye, J., et al., *IgBLAST: an immunoglobulin variable domain sequence analysis tool.* Nucleic Acids Res, 2013. **41**(Web Server issue): p. W34-40.
29. Shakri, A.R., M.M. Rizvi, and C.E. Chitnis, *Development of quantitative receptor-ligand binding assay for use as a tool to estimate immune responses against Plasmodium vivax Duffy binding protein Region II.* J Immunoassay Immunochem, 2012. **33**(4): p. 403-13.
30. Moon, R.W., et al., *Adaptation of the genetically tractable malaria pathogen Plasmodium knowlesi to continuous culture in human erythrocytes.* Proc Natl Acad Sci U S A, 2013. **110**(2): p. 531-6.
31. Adams, J.H., et al., *The Duffy receptor family of Plasmodium knowlesi is located within the micronemes of invasive malaria merozoites.* Cell, 1990. **63**(1): p. 141-53.
32. Gruring, C., et al., *Human red blood cell-adapted Plasmodium knowlesi parasites: a new model system for malaria research.* Cell Microbiol, 2014. **16**(5): p. 612-20.
33. Pain, A., et al., *The genome of the simian and human malaria parasite Plasmodium knowlesi.* Nature, 2008. **455**(7214): p. 799-803.
34. Ord, R.L., et al., *A malaria vaccine candidate based on an epitope of the Plasmodium falciparum RH5 protein.* Malar J, 2014. **13**: p. 326.
35. Douglas, A.D., et al., *Neutralization of Plasmodium falciparum merozoites by antibodies against PfRH5.* J Immunol, 2014. **192**(1): p. 245-58.
36. Saul, A., *Kinetic constraints on the development of a malaria vaccine.* Parasite Immunol, 1987. **9**(1): p. 1-9.
37. Williams, A.R., et al., *Enhancing blockade of Plasmodium falciparum erythrocyte invasion: assessing combinations of antibodies against PfRH5 and other merozoite antigens.* PLoS Pathog, 2012. **8**(11): p. e1002991.
38. Nobrega de Sousa, T., L.H. Carvalho, and C.F. Alves de Brito, *Worldwide genetic variability of the Duffy binding protein: insights into Plasmodium vivax vaccine development.* PLoS One, 2011. **6**(8): p. e22944.
39. Tiller, T., et al., *Efficient generation of monoclonal antibodies from single human B cells by single cell RT-PCR and expression vector cloning.* J Immunol Methods, 2008. **329**(1-2): p. 112-24.
40. Quan, J. and J. Tian, *Circular polymerase extension cloning of complex gene libraries and pathways.* PLoS One, 2009. **4**(7): p. e6441.
41. Wrammert, J., et al., *Rapid cloning of high-affinity human monoclonal antibodies against influenza virus.* Nature, 2008. **453**(7195): p. 667-71.
42. Jin, J., et al., *Accelerating the clinical development of protein-based vaccines for malaria by efficient purification using a four amino acid C-terminal 'C-tag'.* Int J Parasitol, 2017. **47**(7): p. 435-446.

43. Ntumngia, F.B., et al., *Conserved and variant epitopes of Plasmodium vivax Duffy binding protein as targets of inhibitory monoclonal antibodies.* Infect Immun, 2012. **80**(3): p. 1203-8.
44. Hostetler, J.B., et al., *A Library of Plasmodium vivax Recombinant Merozoite Proteins Reveals New Vaccine Candidates and Protein-Protein Interactions.* PLoS Negl Trop Dis, 2015. **9**(12): p. e0004264.
45. Payne, R.O., et al., *Plasmodium vivax Controlled Human Malaria Infection - Progress and Prospects.* Trends Parasitol, 2017. **33**(2): p. 141-150.
46. Miura, K., et al., *Anti-apical-membrane-antigen-1 antibody is more effective than anti-42-kilodalton-merozoite-surface-protein-1 antibody in inhibiting plasmodium falciparum growth, as determined by the in vitro growth inhibition assay.* Clin Vaccine Immunol, 2009. **16**(7): p. 963-8.
47. Kennedy, M.C., et al., *In vitro studies with recombinant Plasmodium falciparum apical membrane antigen 1 (AMA1): production and activity of an AMA1 vaccine and generation of a multiallelic response.* Infect Immun, 2002. **70**(12): p. 6948-60.
48. Smolarek, D., et al., *A recombinant dromedary antibody fragment (VHH or nanobody) directed against human Duffy antigen receptor for chemokines.* Cell Mol Life Sci, 2010. **67**(19): p. 3371-87.
49. Cho, J.S., et al., *Unambiguous determination of Plasmodium vivax reticulocyte invasion by flow cytometry.* Int J Parasitol, 2016. **46**(1): p. 31-9.
50. Russell, B., et al., *A reliable ex vivo invasion assay of human reticulocytes by Plasmodium vivax.* Blood, 2011. **118**(13): p. e74-81.
51. Evans, P., *Scaling and assessment of data quality.* Acta Crystallogr D Biol Crystallogr, 2006. **62**(Pt 1): p. 72-82.
52. McCoy, A.J., et al., *Phaser crystallographic software.* J Appl Crystallogr, 2007. **40**(Pt 4): p. 658-674.
53. Bricogne, *Buster version 2.10.2. Cambridge, United Kingdom: Global Phasing Limited* 2017.
54. Emsley, P., et al., *Features and development of Coot.* Acta Crystallogr D Biol Crystallogr, 2010. **66**(Pt 4): p. 486-501.

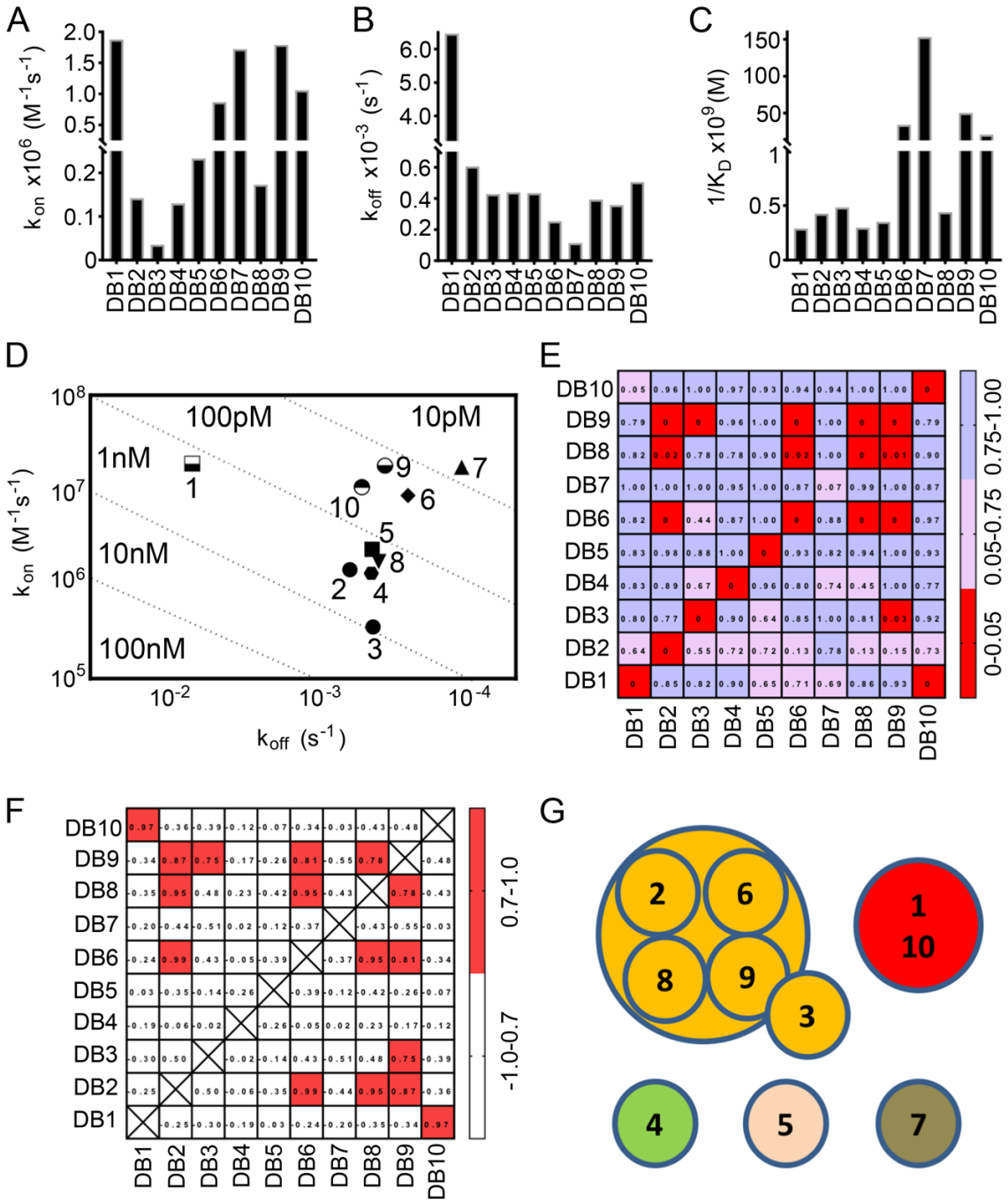

Figure 1: Binding kinetics and epitope bins for the human anti-*Pv*DBPII mAb panel.
Kinetic rate constants of binding for ten human mAbs (DB1-DB10) to *Pv*DBPII as determined by SPR. **(A)** Association rate constant (k_{on}); **(B)** Dissociation rate constant (k_{off}); **(C)** Association constant ($1/K_D$); and **(D)** Iso-affinity plot of k_{on} against the k_{off}. **(E)** A "relative binding" matrix showing the fraction of the second mAb bound to *Pv*DBPII in the presence of bound first mAb. Assays were carried out in both orientations. Boxes are color-coded such that values ≥ 0.75 are in blue, 0.75 > X > 0.05 are in pink and ≤ 0.05 are in red. Negative values were normalised to 0 and values >1 were normalised to 1. **(F)** A "binding profile correlation" matrix showing the Pearson product-moment correlation values of each mAb pair. The correlation threshold was set at 0.7; values equal to or above this are coloured in red as the threshold chosen to represent competition. **(G)** Epitope bins determined from E and F.

A

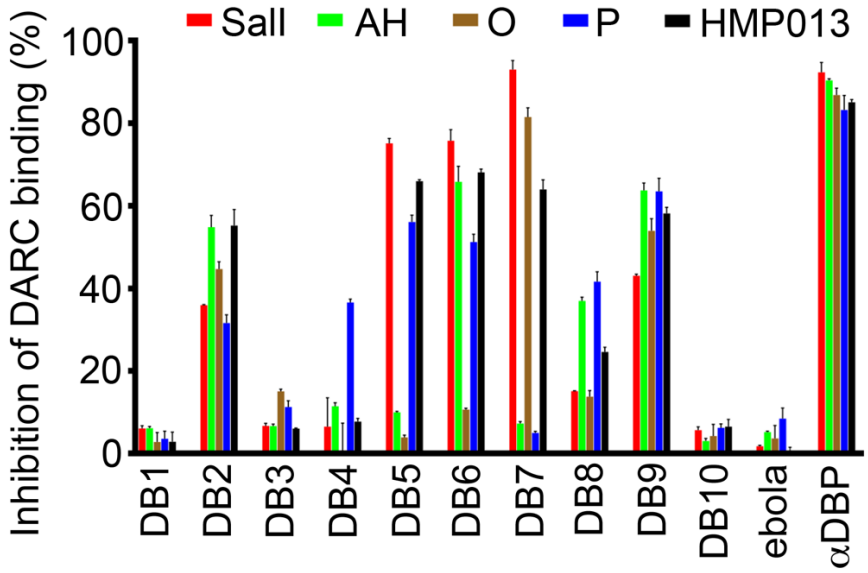

B

AA residue	261	263	288	326	330	339	340	341	345	353	359	372	379	392	402	*	458	464
SalI	F	R	L	K	N	D	E	K	R	S	T	N	L	W	S	–	I	E
P	.	S	F	.	D	G	K	N	H	.	.	K	I	R	.	.	K	.
O	.	S	.	.	.	G	.	.	H	.	.	.	I	.	K	.	.	.
AH	.	S	.	E	.	G	.	Q	.	.	.	K	I	R	.	.	K	.
HMP013	L	S	.	.	.	G	K	N	.	T	R	.	I	.	.	L	.	K

Figure 2: Inhibition of the binding of recombinant *Pv*DBPII to DARC ectodomain.
(A) Assessment of the % binding of five naturally occurring variants of *Pv*DBPII to the DARC ectodomain *in vitro* in the presence of 100 µg/mL concentration of each mAb (DB1-DB10). Individual titration curves are shown in **Figure S1**. "αDBP" is polyclonal human anti-*Pv*DBPII serum at 1:5 dilution while 'ebola' is an anti-*Ebolavirus* recombinant human IgG1 mAb included as a negative control. Data points represent the mean and SD of triplicate test wells. **(B)** Sequence polymorphisms of *Pv*DBPII variants used in the assay. Numbering is according to the SalI reference sequence. Amino acid polymorphisms are indicated for the *Pv*DBPII variants (P, O, AH and HMP013). Amino acids that are the same as the reference sequence are indicated by a full stop, while a hyphen indicates an insertion/deletion and * indicates a leucine insertion between V429 and P430 in HMP013.

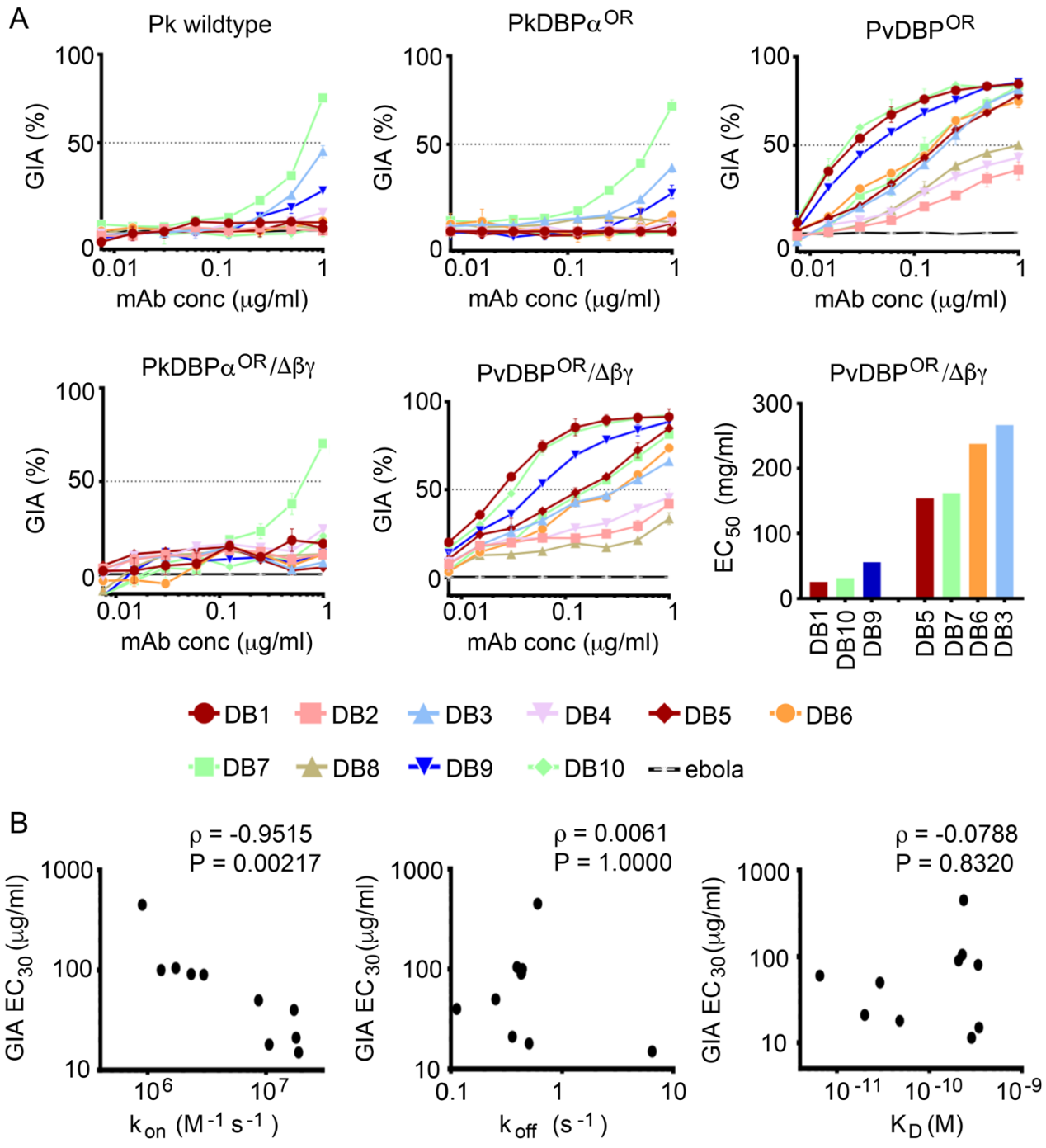

Figure 3: Growth inhibition of transgenic *P. knowlesi* (Pk) lines expressing *Pv*DBP by human mAbs. **(A)** Assays of GIA by the ten anti-*Pv*DBPII human mAbs against five different Pk lines**:** 'Wild type' Pk A1H1; PkDBP^{OR}; PkDBP^{OR}/Δβγ; PvDBP^{OR} and PvDBP^{OR}/Δβγ. Inhibition was tested in a two-fold dilution series starting at 1 mg/mL. Data points represent the mean and SD of triplicate test wells. The EC_{50} values (interpolated by non-linear regression) are shown in ascending rank order for the seven mAbs which reached >50 % GIA against PvDBP^{OR}/Δβγ at the maximum concentration (1 mg/mL). **(B)** k_{on} (on-rate), k_{off} (off-rate) and K_D (dissociation constant), plotted against GIA EC_{30} for PvDBP^{OR}/Δβγ. EC_{30} values were used to include weaker-neutralising mAbs and were interpolated from non-linear regression curves. Kinetic data are as **Figure 1** and **Table S2**. Spearman's rank correlation coefficient (ρ) and *P* value are shown.

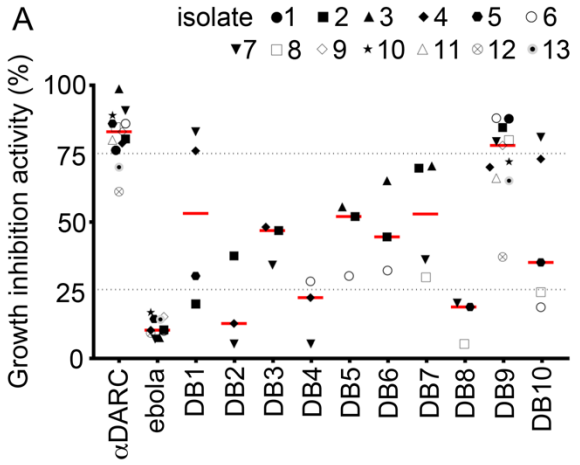

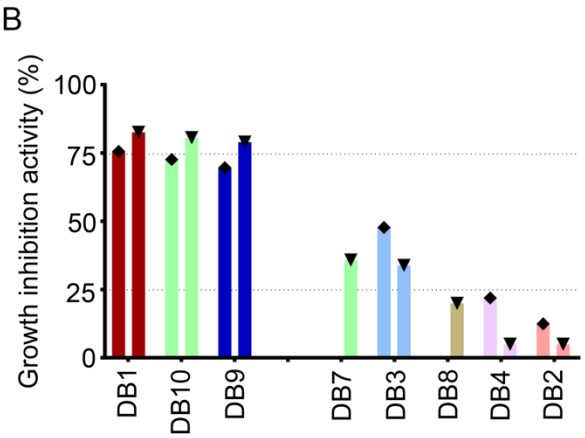

C

Pv isolate	Amino acid residue (position)															
	261	263	288	322	330	339	340	341	345	353	359	372	379	392	*	458
1	.	.	.	.	.	.	.	.	.	.	.	.	I	.	.	.
2	.	.	.	T	.	.	.	.	.	.	.	.	.	.	.	.
3	L	S	.	.	.	G	K	N	H	T	R	.	I	.	.	.
4	.	.	.	.	.	.	.	.	.	.	.	.	.	.	.	.
5	.	.	.	.	.	.	.	.	.	.	.	K	I	R	.	K
6	L	S	.	.	.	G	K	N	H	T	R	.	I	.	L	.
7	.	.	.	.	.	.	.	.	.	.	.	.	.	.	.	.
8	.	S	F	.	D	G	K	N	H	.	.	K	I	R	.	.
Sal I	F	R	L	I	N	D	E	K	R	S	T	N	L	W	-	I

D

Isolate	VHH	EBL	DB1	DB2	DB3	DB4	DB5	DB6	DB7	DB8	DB9	DB10
1	76.2	8.4									87.8	
2	80.4	10.1		37.4	46.7		51.9	44.4	69.3		84.6	
3	98.7	7.3					55.4	65.0	70.4			
4	78.8	10.7	76.1	12.5	48.3	22.6					70.0	73.2
5	82.6	14.2	30.4							18.6		35.3
6	76.9	9.8				28.0	30.8	32.5			88.1	18.5
7	72.8	6.8	83.3	5.9	34.1	5.0			36.3	20.7	79.4	81.1
8	84.7	11.2	19.7						29.5	5.8	80.3	24.7
	% inhibition											

Figure 4: Inhibition of invasion of reticulocytes by Thai *P. vivax* clinical isolates.
(A) *Plasmodium vivax* (Pv) *ex-vivo* invasion assays were performed with thirteen separate isolates of infected blood from local patients. Each data point represents the % inhibition of each antibody against one of the thirteen isolates. All antibodies were tested at a final concentration of 1 mg/mL, except the positive control anti-DARC VHH (αDARC) which was assayed at 25 µg/mL. The red bars represent the median % inhibition for each antibody. A recombinant human IgG1 anti-*Ebolavirus* mAb (ebola) was used as a negative control at 1mg/mL. (B) The most potently inhibitory mAbs against isolate #4 (left hand bar of each pair) and isolate #7 (right hand bar of each pair), the two isolates with SalI vaccine-homologous *Pv*DBPII sequences (**Figure 4C**) to demonstrate correlation with the transgenic Pk assays of GIA **(Figure 3A)**. **(C)** Amino acid polymorphisms found within the *Pv*DBPII gene segment of the eight Thai Pv isolates for which we obtained sequence information. The vaccine homologous Salvador I (SalI) reference sequence is shown in the bottom row. Amino acids that are the same as the reference sequence are indicated by a period, a hyphen indicates an insertion/deletion and * represents a leucine insertion between V429 and P430 in the SalI reference sequence. **(D)** Summary matrix showing the percentage inhibition of invasion by each mAb for each of the sequenced strains. Red represents >65 % inhibition, green represents >30 – 65 % inhibition, and blue represents <30 % inhibition. The positive control was the camelid anti-DARC nanobody (VHH) at 25 µg/mL (αDARC) and the negative control was a recombinant human IgG1 anti-*Ebolavirus* mAb (ebola) at a concentration of 1 mg/mL.

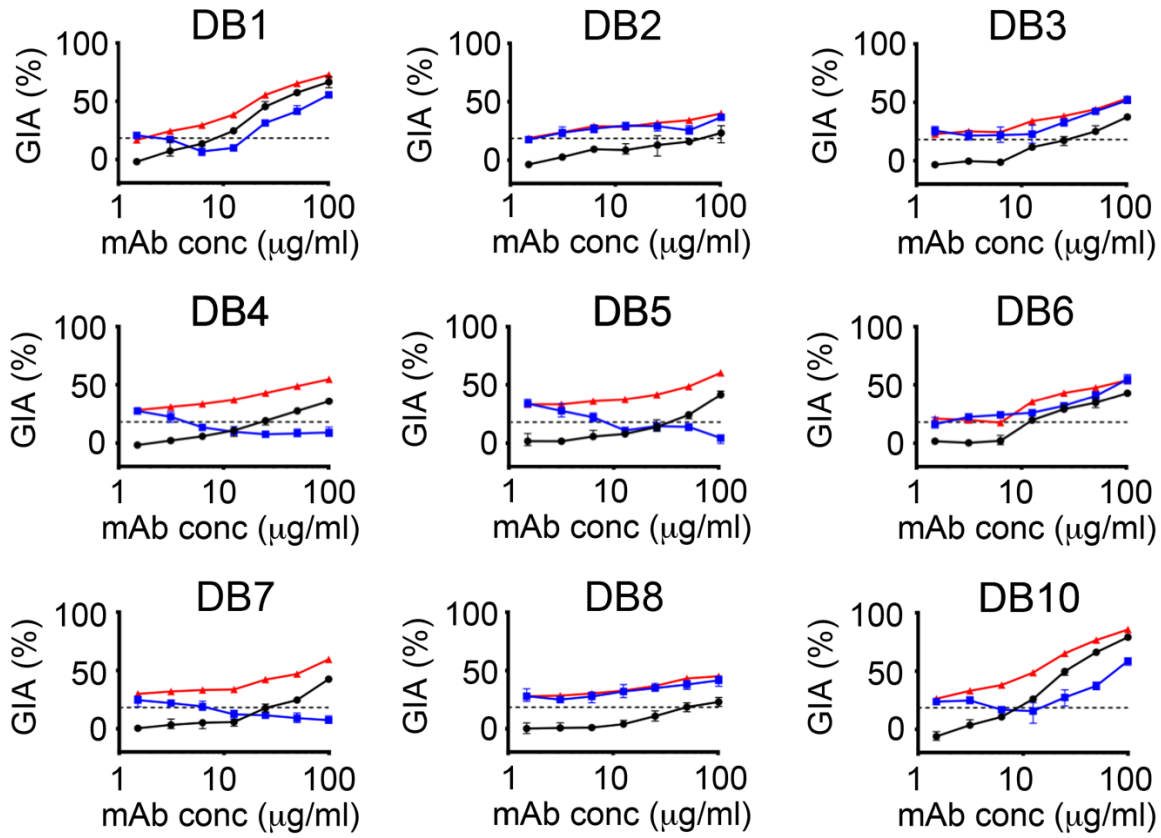

Figure 5: Assessment of synergy, additivity and antagonism by anti-*Pv*DBPII human mAb combinations.

Assays of GIA were performed to assess the effect of other mAb specificities on the inhibitory activity of DB9 against the PvDBP^{OR} transgenic *P. knowlesi* line. DB9 is present and held at a fixed concentration of 25 μg/mL, while the other mAbs are in a two-fold dilution series starting at 100 μg/mL. The black line shows the % inhibition of each mAb in the absence of DB9. The red line shows the predicted additive inhibition ('Bliss additivity' as calculated in the equation in Methods) of the indicated mAb plus DB9 at 25 μg/mL. The blue line shows the actual observed % inhibition of the two combined mAbs. The dotted black line gives the % inhibition of DB9 alone at 25 μg/mL. Data points and error bars represent the mean and standard deviation of triplicate wells.

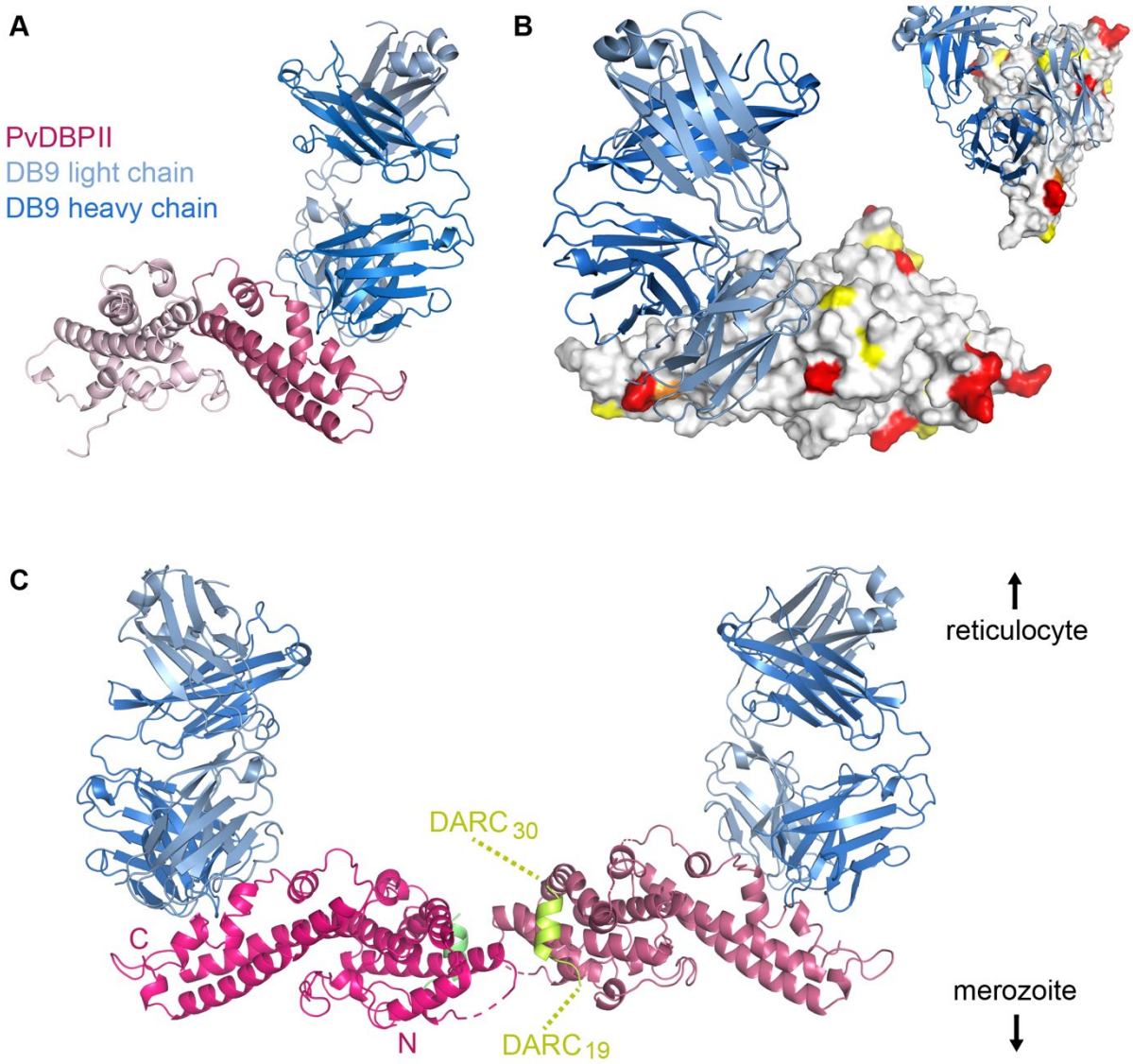

Figure 6: The structural basis for inhibition of *Pv*DBPII by antibody DB9.
(A) The structure of *Pv*DBPII (pink) bound to the Fab fragment of DB9 (blue). *Pv*DBPII is shown in two shades of pink, with subdomains 1 and 2 light pink and subdomain 3 dark pink. DB9 is in two shades with the light chain in light blue and the heavy chain in dark blue. **(B)** *Pv*DBPII is shown in surface representation in grey, with residues known to be polymorphic highlighted according to their sequence entropy (yellow = 0.15-0.3, orange = 0.3-0.45 and red > 0.45). DB9 is in blue, and binds to a conserved region of *Pv*DBPII. **(C)** The structure of *Pv*DBPII:DB9 complex superimposed on the structure of the *Pv*DBPII dimer structure bound to a peptide from the DARC ectodomain, indicating that DB9 may prevent the binding of *Pv*DBP to DARC in the context of the reticulocyte membrane.

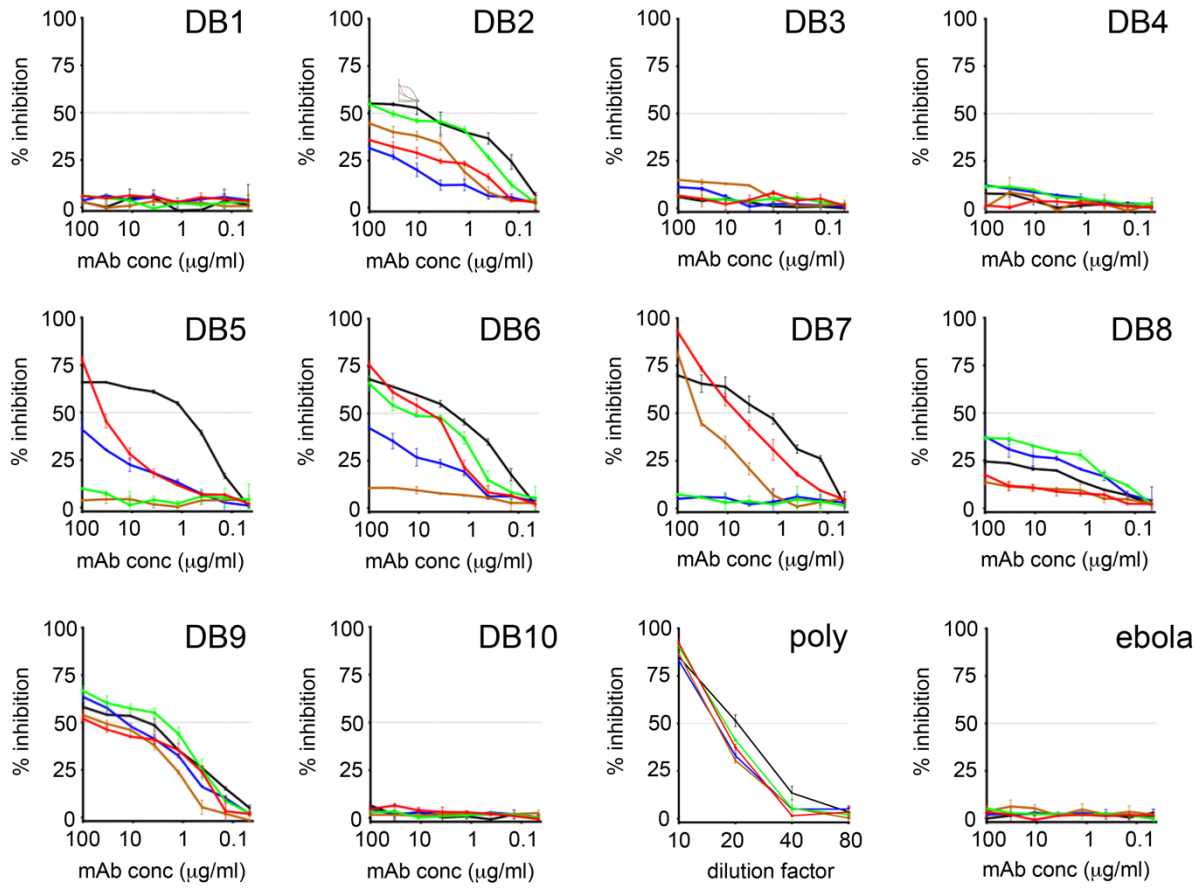

Figure S1: Anti-*Pv*DBPII mAb inhibition of the binding of recombinant *Pv*DBPII variants to the recombinant N-terminal 60 amino acid DARC ectodomain.

The binding of five naturally occurring variants of *Pv*DBPII to the DARC ectodomain in the presence of increasing concentrations of each of DB1-DB10 is shown. The variants are SalI (red), AH (green), O (brown), P (blue) and HMP013 (black). "poly" is polyclonal human anti-*Pv*DBPII serum from the VAC051 clinical trial [19], while "ebola" is an anti-*Ebolavirus* recombinant human IgG1 mAb included as a negative control. Data points represent the mean and SD of triplicate test wells.

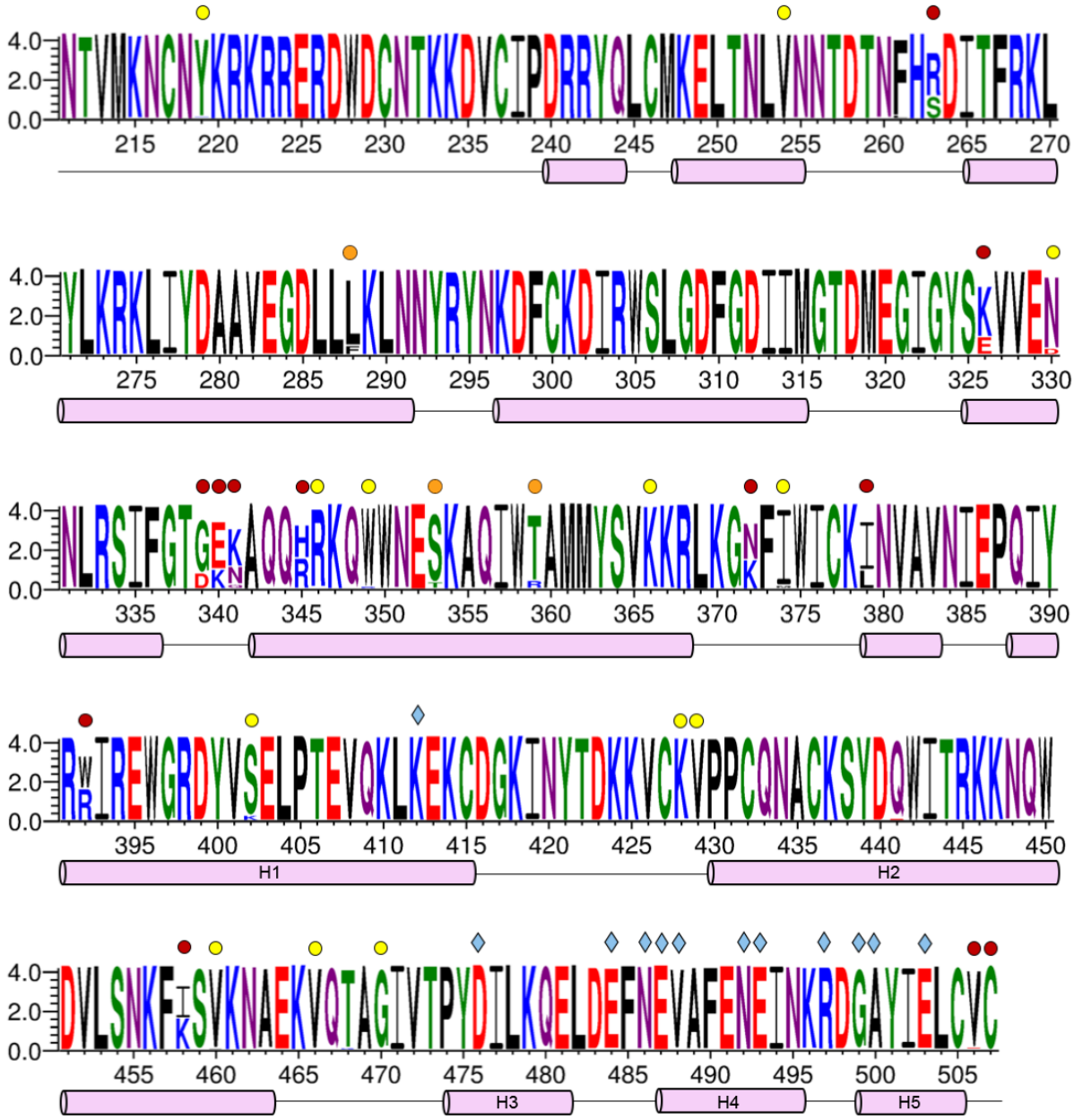

Figure S2: Sequence logo representing sequence conservation across *Pv*DBPII.
Sequence logo derived from 383 sequences of *Pv*DBPII from *P. vivax* isolates. Underneath the logo is the residue number from the SalI *Pv*DBPII variant. Cylinders represent the location of helices while lines represent loops. Above the sequence, blue kites indicate residues which directly contact DB9. Yellow, orange and red circles represent residues with sequence entropies of 0.15-0.3, 0.3-0.45 and >0.45 respectively.

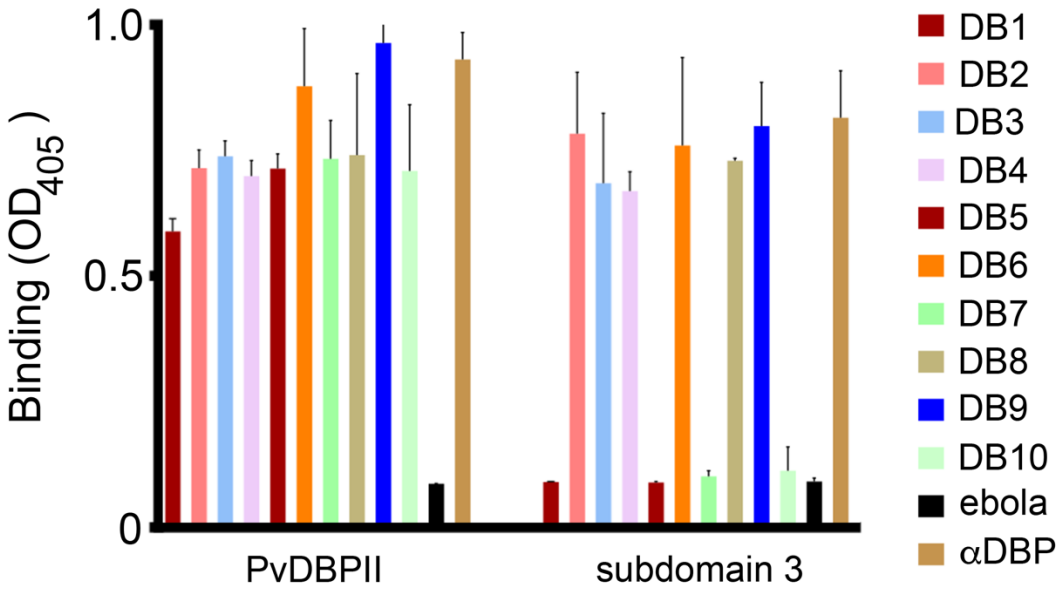

Figure S3: Analysis of the binding of monoclonal antibodies to *Pv*DBPII subdomain 3.
An ELISA of the ten anti-*Pv*DBPII mAbs (at 10 µg/mL) binding to recombinant *Pv*DBPII (left) and subdomain 3 (right). The column heights and error bars represent the mean and SD of triplicate wells. Human polyclonal anti-*Pv*DBPII serum (αDBP) from the VAC051 clinical trial [19] at 1:100 dilution and a human anti-*Ebolavirus* IgG1 mAb (ebola) at 10 µg/mL were used as positive and negative controls, respectively.

Table S1 Genetic lineage of heavy chain variable regions from PvDBPII-specific mAbs. The percentage of nucleotide substitutions relative to germline is shown

mAb	Allele usage	Germline change
DB1	IGHV5-51*03 IGHD3-22*01 IGHJ3*02	1.7% (5/294)
DB2	IGHV4-59*08 IGHD6-13*01 IGHJ3*02	1.4% (4/293)
DB3	IGHV4-31*03 IGHD2-2*01,IGHD2-2*02,IGHD2-2*03 IGHJ4*02	6.4% (19/297)
DB4	IGHV1-69*06 IGHD6-6*01 IGHJ4*02	2.7% (8/295)
DB5	IGHV1-46*03 IGHD1-26*01,IGHD4-11*01,IGHD4-4*01 IGHJ6*02	0.7% (2/296)
DB6	IGHV1-2*02 IGHD3-3*02,IGHD5-12*01,IGHD6-13*01 IGHJ6*02	2.4% (7/294)
DB7	IGHV4-39*01 IGHD3-10*01,IGHD3-10*02,IGHD5-18*01 IGHJ5*02	2.7% (8/298)
DB8	IGHV1-3*01 IGHD6-19*01 IGHJ4*02	2% (6/294)
DB9	IGHV4-39*02 IGHD1-1*01,IGHD1-14*01,IGHD1-20*01 IGHJ2*01	2.3% (7/298)
DB10	IGHV3-21*01 IGHD3-10*01,IGHD3-10*02 IGHJ6*02	2.4% (7/295)

941 ***Table S2 List of anti-PvDBPII mAb binding properties, related to Figure 1 Association-rate (K_{on}),***
942 ***dissociation-rate (K_{off}) and affinity (K_D) are shown.***

mAb	K_{on} ($M^{-1}s^{-1}$)	K_{off} (s^{-1})	K_D (M)
DB1	1.88E+07	6.46E-03	3.44E−10
DB2	9.02E+05	6.05E-04	2.35E−10
DB3	2.98E+06	4.27E-04	2.07E−10
DB4	1.30E+06	4.39E-04	3.37E−10
DB5	2.33E+06	4.33E-04	2.86E−10
DB6	8.65E+06	2.53E-04	2.92E−11
DB7	1.72E+07	1.13E-04	6.55E−12
DB8	1.73E+06	3.92E-04	2.27E−10
DB9	1.79E+07	3.57E-04	2.00E−11
DB10	1.06E+07	5.05E-04	4.78E−11

943

944 ***Table S4: Data collection and refinement statistics***

945

946

	PvDBP:DB9
Data collection	
Space group	$P6_222$
Cell dimensions	
a, *b*, *c* (Å)	173.58, 173.58, 169.88
α, β, γ (°)	90.0, 90.0, 120.0
Wavelength	0.97625
Resolution (Å)	84.94 – 3.04 (3.09 – 3.04)
Total Observations	58086 (2896)
Total Unique	29628 (1442)
R_{pim} (%)	4.0 (46.9)
$CC_{1/2}$	0.999 (0.670)
$I/\sigma(I)$	12.8 (1.2)
Completeness (%)	100.0 (100.0)
Multiplicity	19.6 (20.1)
Refinement	
Number of reflections	30703
R_{work} / R_{free}	17.7 / 22.0
Number of residues	
Protein	648
R.m.s deviations	
Bond lengths (Å)	0.01
Bond angles (°)	1.24
Ramachandran plot	
Favored (%)	95.0%
Allowed (%)	5.0%
Disallowed (%)	0.0%

947 All structures were determined from one crystal.

948 Values in parentheses are for highest-resolution shell.

949

950

951

952

953

954

955

956 **Table S4: List of contacts between *Pv*DBPII and DB9.**

PvDBP-RII residue	Group	Fab Chain	Residue	Group	Interaction
K412	Side Chain	Heavy Chain	Y74	Side Chain	Hydrogen bond
D476	Side Chain	Light Chain	S75	Side Chain	Hydrogen bond
E484	Side Chain	Heavy Chain	E20	Main Chain	Hydrogen bond
E484	Side Chain	Heavy Chain	G45	Main Chain	Hydrogen bond
N486	Side Chain	Heavy Chain	R118	Side Chain	Hydrogen bond
E487	Side Chain	Light Chain	Y68	Side Chain	Hydrogen bond
E487	Side Chain	Light Chain	S75	Main Chain	Hydrogen bond
V488	Side Chain	Light Chain	Y68	Side Chain	Hydrophobic
V488	Side Chain	Light Chain	L74	Side Chain	Hydrophobic
N492	Side Chain	Heavy Chain	T121	Main Chain	Hydrogen bond
E493	Side Chain	Heavy Chain	T52	Side Chain	Hydrogen bond
R497	Side Chain	Light Chain	W51	Side Chain	Cation-pi
R497	Main Chain	Heavy Chain	T121	Side Chain	Hydrogen bond
R497	Side Chain	Heavy Chain	T121	Main Chain	Hydrogen bond
G499	Main Chain	Heavy Chain	T52	Main Chain	Hydrogen bond
A500	Main Chain	Heavy Chain	S51	Main Chain	Hydrogen bond
E503	Side Chain	Heavy Chain	Y54	Side Chain	Hydrogen bond
E503	Side Chain	Heavy Chain	Y79	Side Chain	Hydrogen bond

957 **Table S5: primers**

958

Primer number	Primer sequence (5’ to 3’)
1	ACAGGTGCCCACTCCCAGGTGCAG
2	AAGGTGTCCAGTGTGARGTGCAG
3	CCCAGATGGGTCCTGTCCCAGGTGCAG
4	CAAGGAGTCTGTTCCGAGGTGCAG
5	GGAAGGTGTGCACGCCGCTGGTC
6	ATGAGGSTCCCYGCTCAGCTGCTGG
7	CTCTTCCTCCTGCTACTCTGGCTCCCAG
8	ATTTCTCTGTTGCTCTGGATCTCTG
9	GTTTCTCGTAGTCTGCTTTGCTCA
10	GGTCCTGGGCCCAGTCTGTGCTG
11	GGTCCTGGGCCCAGTCTGCCCTG
12	GCTCTGTGACCTCCTATGAGCTG
13	GGTCTCTCTCSCAGCYTGTGCTG
14	GTTCTTGGGCCAATTTTATGCTG
15	GGTCCAATTCYCAGGCTGTGGTG
16	GAGTGGATTCTCAGACTGTGGTG
17	CACCAGTGTGGCCTTGTTGGCTTG
18	CTTTTTCTAGTAGCAACTGCAACCGGTGTACATTCCGAGGTGCAGCTGGTGCAG
19	CTTTTTCTAGTAGCAACTGCAACCGGTGTACATTCTGAGGTGCAGCTGGTGGAG
20	CTTTTTCTAGTAGCAACTGCAACCGGTGTACATTCCCAGGTGCAGCTGCAGGAG
21	CTTTTTCTAGTAGCAACTGCAACCGGTGTACATTCTGAGGTGCAGCTGTTGGAG
22	CTTTTTCTAGTAGCAACTGCAACCGGTGTACATTCCCAGGTGCAGCTACAGCAGTG
23	CTTTTTCTAGTAGCAACTGCAACCGGTGTACATTCCCAGGTTCAGCTGGTGCAG
24	CTTTTTCTAGTAGCAACTGCAACCGGTGTACATTCCCAGGTCCAGCTGGTACAG
25	CTTTTTCTAGTAGCAACTGCAACCGGTGTACATTCTGAAGTGCAGCTGGTGGAG
26	CTTTTTCTAGTAGCAACTGCAACCGGTGTACATTCCCAGGTACAGCTGCAGCAG
27	CTTTTTCTAGTAGCAACTGCAACCGGTGTACATTCCCAGCTGCAGCTGCAGGAG
28	CTTTTTCTAGTAGCAACTGCAACCGGTGTACATTCTCAGGTGCAGCTGGTGGAG
29	GATGGGCCCTTGGTCGACGCTGAGGAGACGGTGACCAG
30	GATGGGCCCTTGGTCGACGCTGAAGAGACGGTGACCATTG
31	GATGGGCCCTTGGTCGACGCTGAGGAGACGGTGACCGTG
32	CTTTTTCTAGTAGCAACTGCAACCGGTGTACATTCTGACATCCAGATGACCCAGTC
33	CTTTTTCTAGTAGCAACTGCAACCGGTGTACATTCAGACATCCAGTTGACCCAGTCT
34	CTTTTTCTAGTAGCAACTGCAACCGGTGTACATTGTGCCATCCGGATGACCCAGTC
35	CTTTTTCTAGTAGCAACTGCAACCGGTGTACATGGGGATATTGTGATGACCCAGAC
36	CTTTTTCTAGTAGCAACTGCAACCGGTGTACATGGGGATATTGTGATGACTCAGTC
37	CTTTTTCTAGTAGCAACTGCAACCGGTGTACATTCAGAAATTGTGTTGACACAGTC
38	CTTTTTCTAGTAGCAACTGCAACCGGTGTACATTCAGAAATAGTGATGACGCAGTC
39	CTTTTTCTAGTAGCAACTGCAACCGGTGTACATTCAGAAATTGTGTTGACGCAGTCT

40	CTTTTTCTAGTAGCAACTGCAACCGGTGTACATTCGGACATCGTGATGACCCAGTC
41	ATGGTGCAGCCACCGTACGTTTGATYTCCACCTTGGTC
42	ATGGTGCAGCCACCGTACGTTTGATATCCACTTTGGTC
43	ATGGTGCAGCCACCGTACGTTTAATCTCCAGTCGTGTC
44	ATGGTGCAGCCACCGTACGTCTGATTTCCACCTTGGTC
45	CTTTTTCTAGTAGCAACTGCAACCGGTTCCTGGGCCCAGTCTGTGCTGACKCAG
46	CTTTTTCTAGTAGCAACTGCAACCGGTTCCTGGGCCCAGTCTGCCCTGACTCAG
47	CTTTTTCTAGTAGCAACTGCAACCGGTTCTGTGACCTCCTATGAGCTGACWCAG
48	CTTTTTCTAGTAGCAACTGCAACCGGTTCTCTCTCSCAGCYTGTGCTGACTCA
49	CTTTTTCTAGTAGCAACTGCAACCGGTTCTTGGGCCAATTTTATGCTGACTCAG
50	CTTTTTCTAGTAGCAACTGCAACCGGTTCCAATTCYCAGRCTGTGGTGACYCAG
51	GGCTTGAAGCTCCTCACTCGAGGGYGGGAACAGAGTG

959